WATER RESOURCES RESEARCH, VOL. 30, NO. 5, PAGES 1241–1259, MAY 1994

Surface energy balance estimates at local and regional scales using optical remote sensing from an aircraft platform and atmospheric data collected over semiarid rangelands

W. P. Kustas,[1] M. S. Moran,[2] K. S. Humes,[1] D. I. Stannard,[3] P. J. Pinter, Jr.,[2] L. E. Hipps,[4] E. Swiatek,[4] and D. C. Goodrich[5]

Abstract. Remotely sensed data in the visible, near-infrared, and thermal-infrared wave bands were collected from a low-flying aircraft during the Monsoon '90 field experiment. Monsoon '90 was a multidisciplinary experiment conducted in a semiarid watershed. It had as one of its objectives the quantification of hydrometeorological fluxes during the "monsoon" or wet season. The remote sensing observations along with micrometeorological and atmospheric boundary layer (ABL) data were used to compute the surface energy balance over a range of spatial scales. The procedure involved averaging multiple pixels along transects flown over the meteorological and flux (METFLUX) stations. Average values of the spectral reflectance and thermal-infrared temperatures were computed for pixels of order 10^{-1} to 10^{1} km in length and were used with atmospheric data for evaluating net radiation (R_n), soil heat flux (G), and sensible (H) and latent (LE) heat fluxes at these same length scales. The model employs a single-layer resistance approach for estimating H that requires wind speed and air temperature in the ABL and a remotely sensed surface temperature. The values of R_n and G are estimated from remote sensing information together with near-surface observations of air temperature, relative humidity, and solar radiation. Finally, LE is solved as the residual term in the surface energy balance equation. Model calculations were compared to measurements from the METFLUX network for three days having different environmental conditions. Average percent differences for the three days between model and the METFLUX estimates of the local fluxes were about 5% for R_n, 20% for G and H, and 15% for LE. Larger differences occurred during partly cloudy conditions because of errors in interpreting the remote sensing data and the higher spatial and temporal variation in the energy fluxes. Minor variations in modeled energy fluxes were observed when the pixel size representing the remote sensing inputs changed from 0.2 to 2 km. Regional scale estimates of the surface energy balance using bulk ABL properties for the model parameters and input variables and the 10-km pixel data differed from the METFLUX network averages by about 4% for R_n, 10% for G and H, and 15% for LE. Model sensitivity in calculating the turbulent fluxes H and LE to possible variations in key model parameters (i.e., the roughness lengths for heat and momentum) was found to be fairly significant. Therefore the reliability of the methods for estimating key model parameters and potential errors needs further testing over different ecosystems and environmental conditions.

Introduction

In order to quantify the hydrologic cycle over large areas, reliable estimates of regional evapotranspiration (ET) are required. Remote sensing in the optical wavelengths from aircraft [e.g., *Nieuwenhuis et al.*, 1985; *Jackson et al.*, 1987; *Kustas et al.*, 1990] and satellite [e.g., *Carlson et al.*, 1981; *Price*, 1982; *Klassen and van den Berg*, 1985; *Taconet et al.*, 1986; *Kerr et al.*, 1987; *Moran et al.*, 1989; *Brutsaert and Sugita*, 1982] platforms has been used in concert with surface energy balance models for estimating ET from field to regional scales. However, studies which evaluate regional ET cannot easily verify the model output nor validate the remotely sensed data used as model input with ground-based measurements. Instead, comparisons are made with other model computations or by extrapolating point measurements to the area of interest [e.g., *Rambal et al.*, 1985; *Serafini*, 1987; *Nemani and Running*, 1989; *Seguin et al.*, 1989; *Price*, 1990; *Sucksdorff and Ottle*, 1990; *Lagouarde*, 1991].

This deficiency in having ground truth observations over large areas has led to the organization of large-scale field experiments such as the Hydrologic Atmospheric Pilot Ex-

[1]Hydrology Laboratory, Agricultural Research Service, U.S. Department of Agriculture, Beltsville, Maryland.
[2]U.S. Water Conservation Laboratory, Agricultural Research Service, U.S. Department of Agriculture, Phoenix, Arizona.
[3]Water Resources Division, U.S. Geological Survey, Denver, Colorado.
[4]Department of Plants, Soils, and Biometeorology, Utah State University, Logan.
[5]Southwest Watershed Research Center, Agricultural Research Service, U.S. Department of Agriculture, Tucson, Arizona.

Copyright 1994 by the American Geophysical Union.

Paper number 93WR03038.
0043-1397/94/93WR-03038$05.00

Table 1. List of Instruments on Cessna Aircraft Used in This Study

Instrument	Number of Bands	Spectral Range
Exotech radiometer with 15° field of view	4	0.50–0.89 μm (SPOT filters) 0.45–0.90 μm (TM filters)
Everest infrared thermometer (IRT) with 15° field of view	1	8–13 μm

periment and Modélisation du Bilan Hydrique (HAPEX-MOBILHY) [*André et al.*, 1986] and the First International Satellite Land Surface Climatology Project Field Experiment (FIFE) [*Sellers et al.*, 1988]. These experiments were designed to contain an extensive network of ground-based remote sensing observations and measurements of the surface energy balance. In addition, remote sensing data from aircraft and satellite platforms, as well as regional energy flux data, were collected. As a result, the interpretation of the remote sensing data and verification of energy flux estimates over a range of spatial and temporal scales is improving our understanding of the limitations in both modeling and measurement techniques [*Andre et al.*, 1990; *Betts et al.*, 1990; *Carlson et al.*, 1990; *Jacquemin and Noilhan*, 1990; *Mahfouf*, 1990; *Sugita and Brutsaert*, 1990b; *Noilhan et al.*, 1991; *Schmugge et al.*, 1991].

In keeping with the concept of verifying model results, a comparison of modeled and measured energy fluxes over a range of spatial scales was investigated. The data for this analysis were collected during the Monsoon '90 experiment conducted in the Walnut Gulch watershed in southeastern Arizona (31°43'N, 110°W). An overview of the experiment and general description of the watershed is given by *Kustas and Goodrich* [this issue] (see also *Kustas et al.* [1991]). The modeling approach combines remote sensing data from an aircraft platform with ancillary near-surface meteorological data and upper atmospheric boundary layer (ABL) data for computing the surface energy balance components from local to regional scales. The remote sensing data were integrated up from a nominal pixel size of 10^{-1} km to 10^{1} km. The variation in the remotely sensed data as a function of pixel size was quantified. Furthermore, sensitivity of model calculations of the surface energy balance components to remote sensing inputs and other critical model parameters was investigated.

This study differs from *Humes et al.* [this issue (a)] in that Humes et al. extrapolate local surface energy balance components determined at one site to other locations in the basin using only remotely sensed inputs. In the present study, local meteorological and surface roughness parameters were used for each site. Hence in many respects the agreement between fluxes obtained with the local energy balance model and ground truth may be considered optimal for this type of an approach.

The Data

Near-Surface Meteorological and Energy Balance Data

The surface energy balance and ancillary meteorological data were determined at eight locations (meteorological and flux (METFLUX) sites) within the study area. Details of the measurements made and techniques used in computing the surface energy balance are given by *Kustas et al.* [this issue]. The ancillary meteorological data used in this study included wind speed measured at approximately 4.3 m above ground level (AGL), solar radiation, air temperature at ~4 m AGL, and relative humidity. At most of the METFLUX sites the vegetation cover was sparse with shrubs dominating the vegetation type at six of the eight locations. For a thorough description of the soils and vegetation for the study area, see *Schmugge et al.* [this issue] and *Weltz et al.* [this issue], respectively.

Remote Sensing Data

The remote sensing data used in this study were collected by a low-flying Cessna aircraft. (Company and product names are included for the benefit of the reader and do not imply any endorsement by the U.S. government.) On board were nadir-viewing sensors with filters covering the visible, near-infrared and thermal-infrared wavelengths and a video system to record aircraft location. The video system was used to georeference the data. Table 1 gives further details concerning the remote sensing instruments. The aircraft normally flew at an altitude of about 100 m AGL at a nominal air speed of 50 m s^{-1}. The field of view of the instruments was 15°, producing a surface pixel with a diameter of order 25 m at an altitude of 100 m AGL. The instruments were sampled at 1 Hz. This aircraft and instrument package have been used in a number of previous remote sensing experiments [e.g., *Jackson et al.*, 1987; *Moran et al.*, 1989; *Kustas et al.*, 1990].

Figure 1 illustrates the aircraft flight lines and location of the METFLUX sites. Note that lines 1 and 2 traverse the METFLUX sites and Lucky Hills and Kendall subwatersheds where ground-based remote sensing data were collected. A mission usually consisted of flying line 3 several times followed by lines 2 and 1. Lines 1 and 2 would each be flown twice and in opposite directions. A single mission took roughly 30 min to complete, but actual flight time over any of the flight paths normally took less than 5 min. Flight lines 1 and 2 were about 10 km in length, while line 3 was about a 5 km transect. The data collected along lines 1 and 2 are used in the present analysis.

Atmospheric effects on the thermal-IR (IRT) data were estimated using LOWTRAN-7 [*Kneizys et al.*, 1988] and by comparing with ground observations [*Perry and Moran*, this issue]. Also changes in the performance of the IRT instrument due to large differences in ambient and source temperatures were taken into account using laboratory data [*Humes et al.*, this issue (b)]. These factors suggested that the raw IRT temperatures should be increased by roughly 0.5°C. This increase was partially offset by the subtraction of reflected longwave radiation received by the sensor. Finally, the mean emissivity $\varepsilon_s \sim 0.98$ determined for the study area

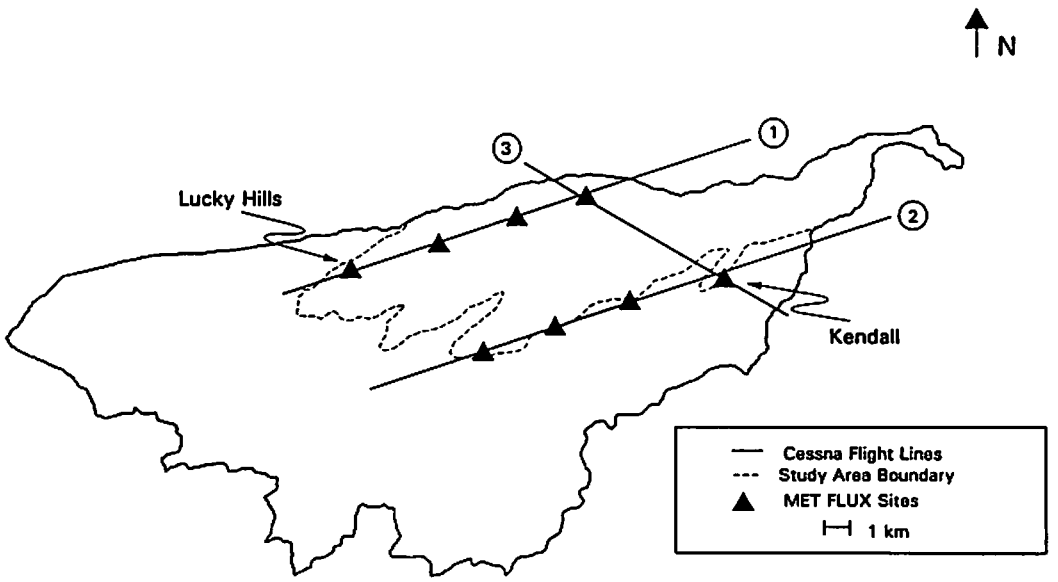

Figure 1. A schematic diagram illustrating approximate locations of the eight METFLUX sites, flight lines for the Cessna aircraft, and the main study area boundary within the Walnut Gulch watershed. Site 1 is located within the shrub-dominated subwatershed, Lucky Hills, and site 5 is within the grass-dominated subwatershed, Kendall. At these two sites, extensive ground-based remote sensing and other geophysical data were collected [*Kustas and Goodrich*, this issue].

resulted in an additional ~0.5°C increase in the raw IRT measurements because the instruments were calibrated with a source emissivity of 0.995. For more details concerning the corrections to the IRT data, see *Humes et al.* [this issue (b)]. The radiance data in the visible and near-infrared (NIR) bands were converted to reflectances by having ground-based instruments with the same band pass filters measuring the radiance from painted $BaSO_4$ panels during the aircraft overpass.

Examples of surface temperature and near-infrared over red reflectance (NIR/red) for flights on day of year (DOY) 209 and DOY 216 are shown in Figures 2 and 3. For both days the variation in surface temperature between adjacent pixels is typically ±2 K with variations of ±4 K commonly observed within a 2-km segment. For DOY 209, line 2 tends to have higher surface temperature values than line 1 while the NIR/red ratio plotted in Figure 3 does not indicate a significant difference in reflectance. For DOY 216, differences in surface temperature values between the flight lines are not as consistent as DOY 209, and there is much larger variability in the NIR/red ratio. This is probably due to the effects of clouds developing in the region during the overflight (see the analysis section). In comparing the remote sensing data from DOY 209 and 216 the most striking features are the higher surface temperatures observed for DOY 209 and the larger and more spatially variable NIR/red ratio for DOY 216. Reasons for these differences can be explained by the environmental conditions present during these two days (see below).

Atmospheric Boundary Layer Data

On selected days, tethered and free soundings provided air temperature, water vapor content, wind speed, and direction for the lower troposphere. The launch site was normally at Lucky Hills; however, a second system made tethered sonde releases around the Kendall subwatershed for studying advection (see Figure 1). More details concerning the atmospheric boundary layer (ABL) data are given by *Hipps et al.* [this issue]. The tethered system gave detailed profiles (~10 m intervals) up to 500–600 m AGL, while the coarser resolution of the free soundings (~40 m intervals) went up to 4000–5000 m AGL. A typical profile of potential temperature and wind speed during daytime convective conditions is shown in Figure 4 for one of the free soundings. Notice in Figure 4a a fairly uniform profile in potential temperature (±0.5 K) from roughly 10^2 m to 10^3 m AGL which is capped by a strong inversion layer. The wind profile over this same depth (Figure 4b) is fairly noisy, possibly due to strong convective eddies affecting the flow.

The Model

The objective of this study was to employ a model for computing energy fluxes over a range of spatial scales specified by the pixel resolution of the remotely sensed data. An attempt was made to minimize the number of required inputs to run the model, yet maintain a physically based approach. The ultimate goal is to have an operational model for estimating energy fluxes over a range of length scales. The primary boundary condition in the model is the surface energy balance,

$$R_n + G + H + LE = 0, \qquad (1)$$

where R_n is the net radiation, G the soil heat flux, H the sensible heat flux, and LE the latent heat flux, all in watts per square meter. Energy due to photosynthesis and stored inside the canopy is neglected. In (1), fluxes away from the surface are negative while fluxes toward the surface are positive. The net radiation is the difference between incoming and outgoing radiant fluxes integrated over all wavelengths, i.e.,

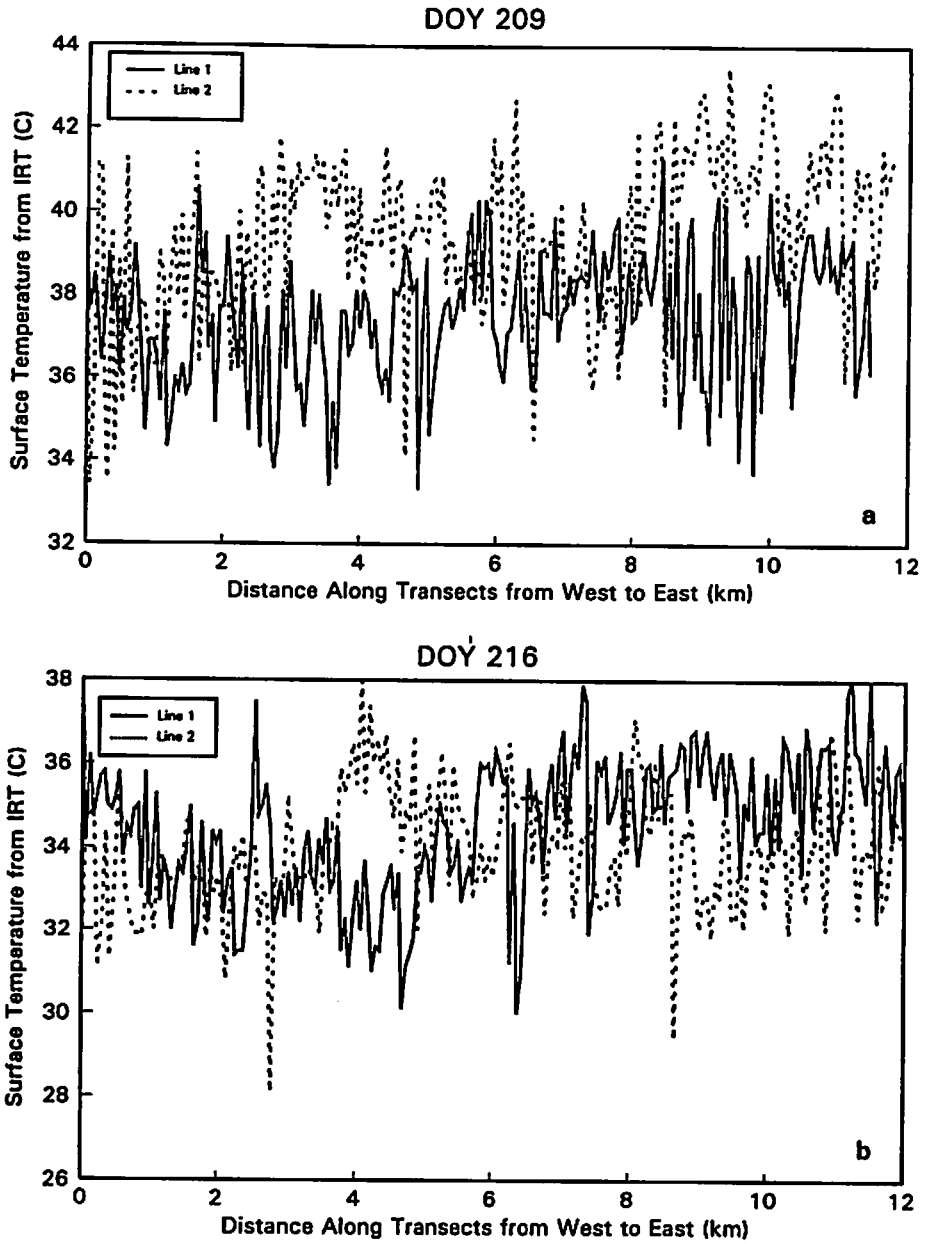

Figure 2. Surface temperature observations from the aircraft-mounted IRT flying lines 1 and 2 (see Figure 1) during (a) DOY 209 at ~1030 MST and (b) DOY 216 at ~1100 MST.

$$R_n = R_{si} + R_{Li} + R_{so} + R_{Lo}. \quad (2)$$

The subscript s and L represent shortwave (0.15–4.0 μm) and longwave (>4 μm) radiation, respectively, and subscript i and o signify incoming and outgoing radiation. Recent reviews of techniques using geostationary satellites for estimating the components in (2) are given by *Pinker* [1990] and *Sellers et al.* [1990]. The method used in this paper combines local meteorological observations for estimating the incoming components in (2), while the outgoing components are estimated with remote sensing data [*Jackson*, 1985]. Thus the radiation balance given by (2) was rewritten as

$$R_n = (1 - \alpha)R_{si} + \varepsilon_s \varepsilon_a \sigma T_a^4 - \varepsilon_s \sigma T_s^4 \quad (3)$$

where α is the surface albedo, σ the Stefan-Boltzmann constant (5.67×10^{-8} W m^{-2} K^{-4}), T_a the near-surface air temperature (kelvins), T_s the surface temperature observed by the radiometer (kelvins), and ε the emissivity with the subscripts s and a signifying the surface and atmosphere, respectively. The value of α was estimated using a weighted sum of the spectral reflectance factors for bands in the visible and near-infrared wavelengths [*Brest and Goward*, 1987]. For vegetated surfaces,

$$\alpha = 0.526(\text{VIS}) + 0.418(\text{NIR}), \quad (4)$$

where VIS is the visible reflectance factor, usually in the red wavelength, and NIR is the near-infrared reflectance factor. For sparsely vegetated surfaces or bare soil, which was assumed when the NIR/red ratio vegetation index [*Tucker*, 1979] fell below 1.5, the relationship is

$$\alpha = 0.526(\text{VIS}) + 0.474(\text{NIR}) \quad (5)$$

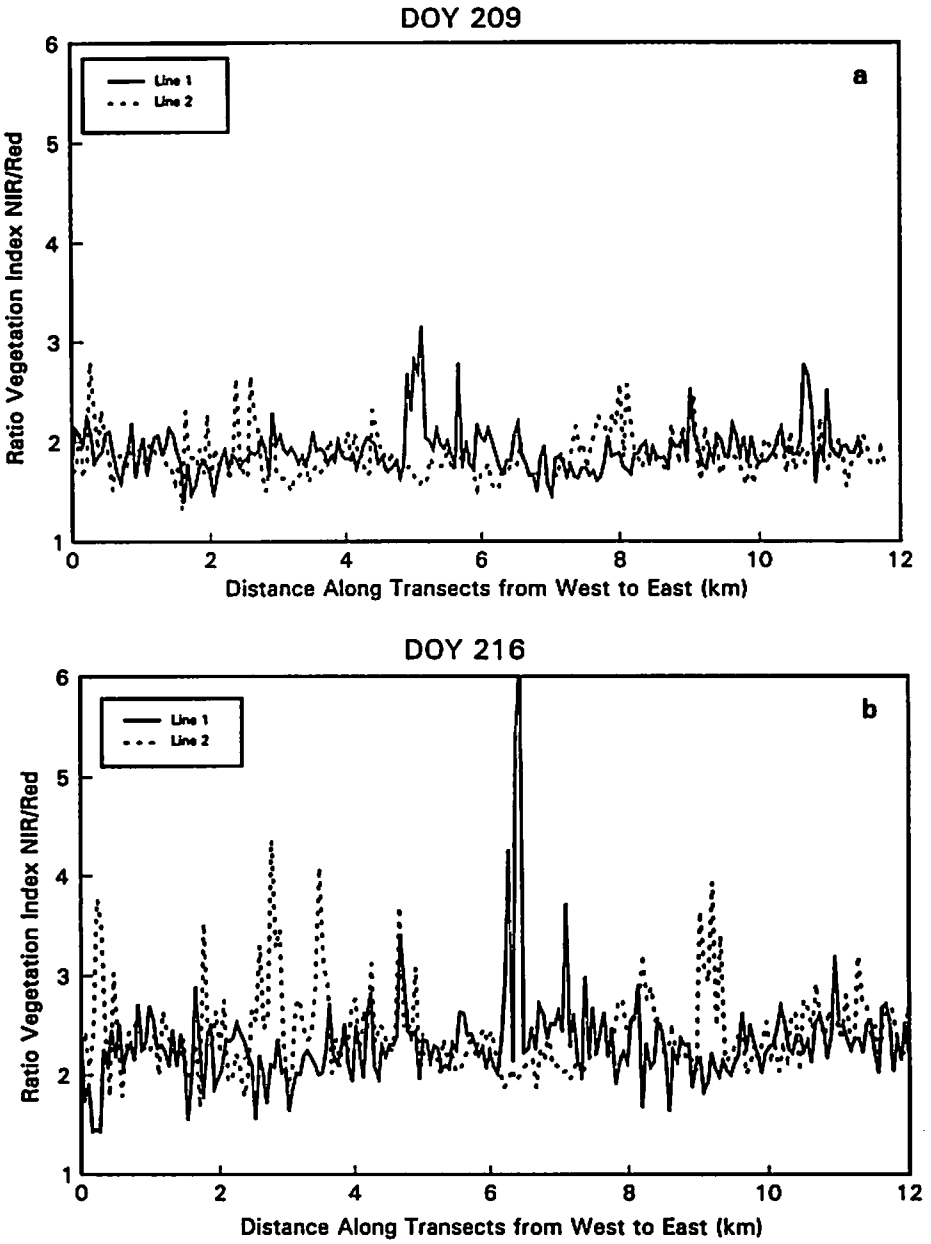

Figure 3. Same as Figure 2, except plots are of the ratio vegetation index, NIR/red, estimated from the multispectral radiometer on board the aircraft.

Since nadir reflectance measurements were used in the present study, the albedo estimate was not representative of hemispherical reflectance [*Kimes et al.*, 1980]. Simplified methods to convert nadir to hemispherical reflectance estimates have been developed [e.g., *Walthall et al.*, 1985], but have not been calibrated for heterogeneous surfaces such as semiarid rangelands. The emissivity of the atmosphere under clear skies was estimated using a physically based expression from *Brutsaert* [1975],

$$\varepsilon_a = 1.24(e_0/T_a)^{1/7}, \tag{6}$$

where e_0 is the near-surface vapor pressure (10^2 Pa). Adjustment to ε_a for the effects of clouds was considered minor compared to the impact of clouds on R_{si} (see Figure 7). The value of ε_s was determined using an approach outlined by *Fuchs and Tanner* [1966], and results are given by *Humes et al.* [this issue (b)]. In future work on regional energy balance studies, methods will be adopted that use remote sensing from satellites to infer incoming radiation [e.g., *Pinker et al.*, this issue].

The soil heat flux can be solved numerically as a function of the thermal conductivity of the soil and the vertical temperature gradient [e.g., *Camillo et al.*, 1983]. This approach may be difficult to apply over large heterogeneous areas; however, attempts at using routine weather data with a physically based model may have operational capabilities [*Camillo*, 1989]. A simplified approach adopted for present study allows G to be determined primarily from remote sensing information. It is derived from experimental observations that the ratio G/R_n is relatively constant for a period surrounding midday and varies primarily as a function of amount of vegetation cover [*Clothier et al.*, 1986; *Choudhury*

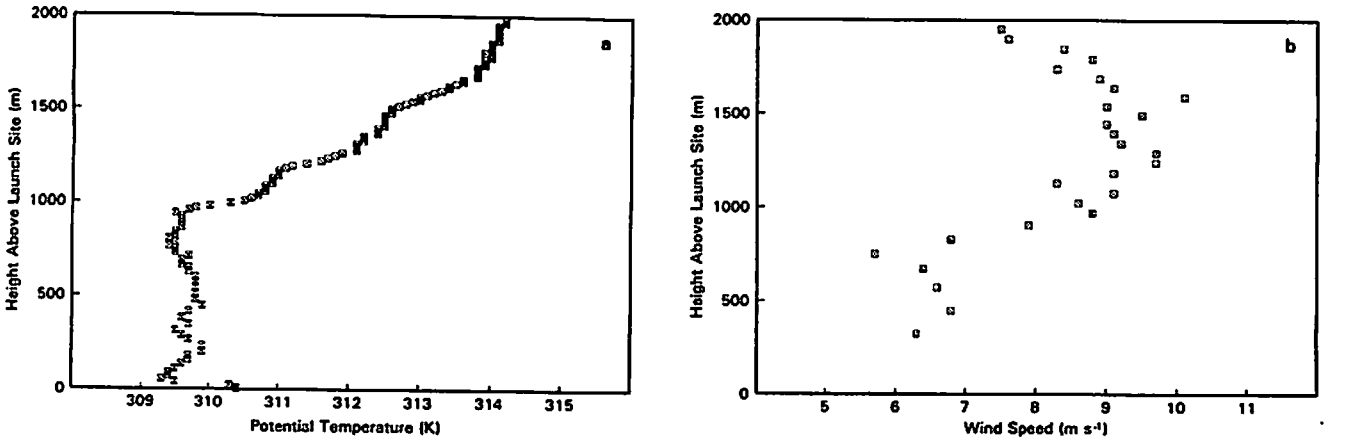

Figure 4. Atmospheric boundary layer profiles of (a) potential temperature and (b) wind speed under daytime convective conditions.

et al., 1987; *Kustas and Daughtry*, 1990]. The amount of vegetation cover can be quantified by vegetation indices [*Tucker*, 1979; *Tucker and Sellers*, 1986]. Problems with such a simple parameterization are associated with the temporal hysteresis in G/R_n [*Moran et al.*, this issue] and the effects of soil moisture on the magnitude of G/R_n [*Brutsaert*, 1982]. Simplified techniques to adjust G/R_n for hysteresis [*Camuffo and Bernardi*, 1982] and soil moisture [*Owe and van de Griend*, 1990] may be applicable; nevertheless, it was felt that these factors are secondary to the effect of the amount of vegetation cover on the magnitude of G/R_n for large-area estimates. The relationship from *Kustas and Daughtry* [1990, Table 1a]

$$-G/R_n = 0.36 - 0.02\text{NIR/red} \tag{7}$$

was used in the present study. The effects of soil background, look angle and solar zenith angle can significantly alter vegetation indices, especially for arid and semiarid ecosystems [*Huete and Jackson*, 1987; *Tueller and Oleson*, 1989]. But these effects are not considered significant enough to influence the estimate of G/R_n as evaluated by (7).

The sensible heat flux was evaluated using a bulk resistance approach [*Monteith*, 1973],

$$H = -\rho C_p(\theta_s - \theta_a)/r_{ah}, \tag{8}$$

where ρ is the air density (kilograms per cubic meter), C_p the specific heat at constant pressure (J kg^{-1} K^{-1}), θ_s the surface potential temperature (kelvins), θ_a the potential temperature at a reference height z_θ in the atmosphere, and r_{ah} the bulk resistance to heat transfer across the surface-atmosphere interface (seconds per meter). The magnitude of r_{ah} depends upon reference height where wind speed and air temperature are measured, momentum and scalar roughness parameters, atmospheric stability, and the wind speed. If θ_a and u are measured in the surface layer, the bulk resistance expression

$$r_{ah} = \{\ln[(z_u - d_{0m})/z_{0m}] - \Psi_m\}\{\ln[(z_\theta - d_{0h})/z_{0m}] + \ln(z_{0m}/z_{0h}) - \Psi_h\}/(k^2u) \tag{9}$$

requires the estimation of several parameters.

The symbols d_{0m}, z_{0m}, d_{0h}, and z_{0h} are the displacement height and roughness lengths for momentum and heat in meters, respectively. The symbol k (~0.4) is von Karman's constant and u (meters per second) is the wind speed at reference height z_u. Finally, Ψ_m and Ψ_h represent the stability corrections functions for wind and temperature.

During convective daytime conditions the surface layer composes about the first 10% of the ABL [*Stull*, 1988]. Over this depth in the ABL, application of Monin-Obukhov similarity theory is shown to satisfactorily describe the flux-profile relationships for wind, potential temperature, and specific humidity even for hilly terrain [*Brutsaert and Sugita*, 1990]. Various functional forms of the stability correction functions for unstable conditions are available. A recent review by *Högström* [1988] suggests that the Businger-Dyer formulations [e.g., *Dyer*, 1974] give satisfactory results in the unstable surface layer where

$$\Psi_m = 2\ln[(1+x)/2] + \ln[(1+x^2)/2] - 2\arctan(x) + \pi/2 \tag{10a}$$

$$\Psi_h = 2\ln[(1+x^2)/2] \tag{10b}$$

The symbol $x = [1 - 16(z - d_{0m})/L]^{1/4}$ and L is the Obukhov length [*Monin and Obukhov*, 1954] given by

$$L = u_*^3/[k(g/T_a)(H_v/\rho C_p)], \tag{11}$$

where $u_* = (\tau/\rho)^{1/2}$ (meters per second) is the friction velocity (τ is the surface shear stress), g the acceleration of gravity (m s^{-2}), $H_v = (H + 0.61T_aC_pE)$ is the virtual sensible heat flux, and E is the rate of surface evaporation (kg m^{-2} s^{-1}). Equations (10a) and (10b) are integral forms of the Monin-Obukhov similarity correction functions and neglect the lower limit of integration at z_{0m} and z_{0h} [*Paulson*, 1970]. Under highly unstable conditions, where $-(z - d_{0m})/L > 10^1$, theoretical and experimental evidence suggests that significantly different forms of the surface layer stability correction functions are required [*Carl et al.*, 1973; *Kader and Yaglom*, 1990]. However, in the present study, surface layer values of $-(z - d_{0m})/L$ were of order 10^{-1}.

The difference between d_{0m} and d_{0h} was neglected because there is little experimental evidence suggesting that separate values of displacement heights for scalars and

momentum are necessary [*Kustas*, 1990]. On the other hand, there is both theoretical and experimental evidence showing a significant difference in the values of scalar versus momentum roughness. The distinction in roughness lengths for heat and momentum mainly stems from differences in transfer processes near the surface [*Thom*, 1972]. The logarithm of the ratio z_{0m} to z_{0h} in the bulk resistance expression (9) represents the quantity kB^{-1} ($\equiv \ln (z_{0m}/z_{0h})$) which was studied in detail by earlier investigators [e.g., *Owen and Thomson*, 1963; *Chamberlain*, 1968; *Garratt and Hicks*, 1973]. For many vegetated surfaces both theoretical and experimental studies show that kB^{-1} is of order 2. But for roughness elements considered "bluff body" (e.g., furrowed fields, cylinders in wind tunnels) values of kB^{-1} are found to be considerably larger [*Garratt and Hicks*, 1973; *Kustas*, 1990]. For sparse canopy covered surfaces with dry soil, values of kB^{-1} were found to be of the same order of magnitude as those observed for bluff body surfaces [*Kustas et al.*, 1989b]. Similar results were obtained in recent studies over complex terrain where kB^{-1} values ranged from order 4 to 10 [*Beljaars and Holtslag*, 1991; *Sugita and Brutsaert*, 1990b]. It must be emphasized that the magnitude of kB^{-1} determined with a radiometric surface temperature is dependent on the look angle of the sensor and on the solar zenith angle [*Kimes*, 1980; *Huband and Monteith*, 1986; *Brunet et al.*, 1991; *Sugita and Brutsaert*, 1990b]. But to account for these effects is not straightforward and would require measurements at multiple view angles to evaluate the effect. Thus in keeping with the goal of having an operational model, a simple empirical expression for kB^{-1},

$$kB^{-1} = s_{kB}u(\theta_s - \theta_a), \tag{12}$$

derived from data collected over another semiarid region was used [*Kustas et al.*, 1989b]. The slope in the kB^{-1} equation, s_{kB}, is approximately 0.17 s m^{-1} K^{-1}.

The local momentum roughness length and displacement height required in (9) when using near-surface measurements were determined for some of the sites using several techniques. For the two main study areas, Lucky Hills and Kendall (sites 1 and 5), wind profile measurements at four or five levels were used with an iterative least squares technique to determine z_{0m} and d_{0m} [*Kustas et al.*, 1989a; *Robinson*, 1962]. Another approach utilized the standard deviation of the vertical velocity, σ_w, along with measurements of the turbulent fluxes H and LE and a measurement of near-surface wind speed with assumed values of z_{0m} and d_{0m} for computing u_* [*Weaver*, 1990]. For more details of the methods used in estimating z_{0m} and d_{0m}, see *Kustas et al.* [this issue]. A remote sensing method which utilizes airborne laser altimeter data shows some promise in obtaining reliable estimates of z_{0m}. This technique is described by *Menenti and Ritchie* [this issue].

For larger-scale estimates of H, values of temperature and wind speed at heights $(z - d_{0m}) \sim 10^1$ m have been utilized [e.g., *Klassen and van den Berg*, 1985]. To obtain regional estimates of H which are representative of integrated values over length scales of order 10^1 km, values of wind speed and temperature are needed at heights $(z - d_{0m}) \sim 10^2$ m. The upper limit of the validity of the surface layer formulations (8)–(11) in terms of $(z - d_{0m})/z_{0m}$ for complex terrain is found to be around 100 to 150 by *Brutsaert and Sugita* [1990]. But *Brutsaert and Sugita* [1990] discovered that the region of validity is highly variable and often difficult to establish by merely inspecting the radiosonde profiles. Therefore an alternative approach was adopted which uses average wind speed and potential temperature measurements in the convective mixed layer. This yields [cf. *Kustas et al.*, 1989a]

$$R_{ah} = \{\ln [(H_i - D_{0m})/Z_{0m}] + \ln (Z_{0m}/Z_{0h}) - C\} \cdot \{\ln [(H_i - D_{0m})/Z_{0m}] - B\}/(k^2U) \tag{13}$$

which is a bulk resistance expression for the ABL. The symbol H_i is the height of the top of the mixed layer, Z_{0m} and Z_{0h} are the regional roughness lengths for momentum and heat, respectively, C and B are similarity stability functions for heat and momentum, respectively, D_{0m} is the regional scale displacement height, and U is the average mixed layer wind speed. Early studies have shown that this bulk similarity approach for momentum and heat transfer in the convective ABL works reasonably well under general atmospheric conditions [e.g., *Garratt and Francey*, 1978; *Garratt et al.*, 1982]. The bulk ABL resistance expression

$$H = -\rho C_p(\Theta_s - \Theta_a)/R_{ah} \tag{14}$$

is similar to the surface layer equation (compare (8)) but has Θ_s representing a large-area estimate of surface potential temperature and Θ_a as the average mixed layer potential temperature. The functional forms of the stability functions C and B were taken from a recent study by *Brutsaert and Sugita* [1991]. The logarithmic form of the expressions for B,

$$B = 0.54 \ln [(H_i - D_{0m})/L] + 2.3, \tag{15}$$

and C,

$$C = 0.4 \ln [(H_i - D_{0m})/L] + 4.4, \tag{16}$$

were adopted. The coefficients in (15) and (16) are averages from the results given by *Brutsaert and Sugita* [1991].

From tower data [e.g., *Korrell et al.*, 1982], estimates of a regional or effective roughness [*Fiedler and Panofsky*, 1972] reveal significant differences with the local roughness. This has even been observed over surfaces containing little variation in topography [*Beljaars*, 1982]. When tower data are not available, other methods have been developed. These include the use of a normalized standard deviation of wind speed from wind stations [*Wieringa*, 1980, 1986], neutral wind profiles from radiosondes in the lower ABL [e.g., *Nappo*, 1977; *Thompson*, 1978; *Kustas and Brutsaert*, 1986; *Parlange and Brutsaert*, 1989; *Sugita and Brutsaert*, 1990a], and semiempirical formulas developed from numerical and experimental studies of flow over varying density of roughness features [e.g., *Lettau*, 1969; *Mason*, 1988; *Taylor et al.*, 1989]. Unfortunately, few modeling studies attempt to compare their results with observations [e.g., *Emeis*, 1987]. Since neutral wind profile observations under stationary conditions in the ABL are rare and their analysis over hilly terrain is complicated [e.g., *Sugita and Brutsaert*, 1990a], it was decided to use several semiempirical formulas requiring knowledge of only gross features of the surface. The equation proposed by *Taylor et al.* [1989],

$$\ln (Z_{0m}/z_{0m}) = 3.5(h2\pi/\lambda)^2 \ln (\lambda/z_{0m}) \tag{17}$$

was employed. In (17), h is the mean amplitude or height of the obstacles, λ is the wavelength of the obstacle (assuming

Table 2. Description of Environmental Conditions in the Study Area for DOY 209, 216, and 221

DOY	Sky Condition	Soil Moisture	Vegetation
209	clear	dry soil surface, but adequate soil moisture in root zone	unstressed
216	partly cloudy	relatively high moisture content from the surface to the root zone	unstressed
221	partly cloudy	nonuniform drying of near-surface soil moisture over the METFLUX network	unstressed

DOY denotes day of year.

sinusoidal topography), and z_{0m} refers to the roughness length that the surface would have without orographic features. Another formulation is given by *Emeis* [1987] where

$$\ln (Z_{0m}/z_{0m}) = 40h/\lambda \tag{18}$$

Emeis [1987] also adapted *Lettau*'s [1969] expression for his two-dimensional study with a sinusoidal surface yielding

$$Z_{0m} = 0.5h^2/\lambda \tag{19}$$

Equations (17)–(19) for estimating Z_{0m} require mean height of the obstacles and average obstacle spacing, while (17) and (18) need an estimate of z_{0m}. Preliminary estimates of Z_{0m} were also obtained with the airborne laser altimeter data using a similar approach [*Menenti and Ritchie*, this issue]. For Z_{0h}, as a working hypothesis the same empirical expression for kB^{-1} was used with the ABL data, namely,

$$kB^{-1} = s_{kB}U(\Theta_s - \Theta_a) \tag{20}$$

Data Analysis

For three days (DOY 209, 216, and 221) with different meteorological and soil moisture conditions, aircraft and atmospheric boundary layer data were collected under mostly clear skies. Table 2 gives a qualitative description of environmental conditions that prevailed for each day. A

Table 3. Daytime Average (Over the Period 0700–1800 MST) of the Surface Energy Balance Components, Wind Speed, Wind Direction, and Air Temperature and Daily Gravimetric Soil Moisture and the Midday Bowen Ratio, B_0, Averaged for the Period 1030–1430 MST

Site	R_n, W m^{-2}	G, W m^{-2}	H, W m^{-2}	LE, W m^{-2}	B_0 (H/LE)	u, m s^{-1}	T_a, °C	WD, deg from N	Soil Moisture, % by volume
					DOY 209				
1	405	−112	−113	−180	0.70	3.36	29.0	284	2.7
2	407	−86	−108	−213	0.50	3.48	28.9	300	4.2
3	379	−111	−111	−157	0.78	3.39	28.4	294	2.4
4	437	−95	−116	−226	0.50	4.03	27.8	278	3.0
5	434	−92	−150	−192	0.60	4.02	27.7	303	3.3
6	401	−83	−133	−185	0.81	3.46	28.5	303	2.1
7	390	−91	−121	−178	0.74	2.98	29.0	304	2.4
8	444	−117	−105	−223	0.56	2.92	28.1	303	3.2
					DOY 216				
1	419	−114	−77	−238	0.30	2.34	26.9	114	12.1
2	405	−93	−86	−229	0.34	2.51	26.7	126	13.1
3	381	−120	−70	−197	0.38	2.64	26.2	126	11.2
4	433	−109	−97	−231	0.42	2.87	25.7	114	13.0
5	434	−110	−96	−238	0.38	3.02	25.8	152	13.4
6	412	−102	−112	−209	0.57	2.63	26.4	124	11.7
7	424	−85	−86	−261	0.35	2.31	26.8	144	10.6
8	477	−110	−77	−302	0.26	2.46	25.3	110	13.2
					DOY 221				
1	396	−106	−143	−148	1.1	4.84	27.6	107	3.6
2	410	−84	−132	−194	0.73	5.04	27.3	122	7.5
3	384	−108	−112	−164	0.82	4.79	26.7	117	7.0
4	419	−97	−112	−211	0.54	6.32	25.9	108	7.4
5	422	−90	−134	−209	0.70	6.35	25.9	116	7.8
6	399	−89	−127	−189	0.79	4.53	26.8	118	7.2
7	384	−73	−128	−183	0.83	4.39	27.3	124	2.3
8	421	−100	−153	−169	1.12	4.66	26.3	117	3.9

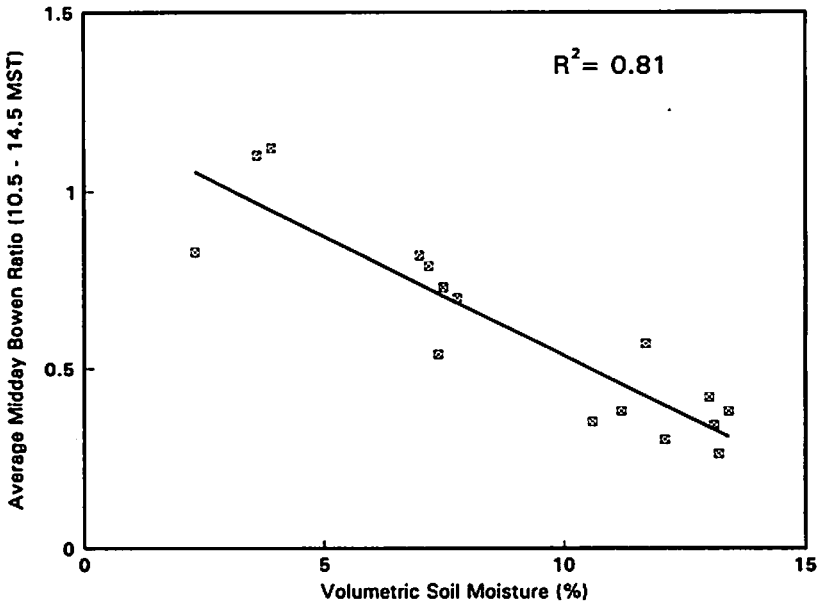

Figure 5. Relation between volumetric soil moisture for the 0–5 cm soil layer and midday (1030–1430 MST) Bowen ratio from the METFLUX network for DOY 216 and 221.

significant amount of precipitation fell in early July before the field campaign, which led to an early green-up in the vegetation. There was a 6-day period before DOY 209 with negligible precipitation, resulting in a significant drying of the soil surface (0–5 cm depth). The period of drying continued until several rain events on DOY 213, 214, and 215 supplied significant moisture to the upper soil layer for most of the study area [see *Schmugge et al.*, this issue; *Goodrich et al.*, this issue]. However, there was significant spatial variation in rainfall amounts over the watershed. This was followed by a period of drying, which was interrupted briefly by a small amount (1–3 mm) of precipitation falling over most of the watershed on DOY 218.

Table 3 lists the daytime energy balance components in watts per square meter, wind speed, wind direction and air temperature averaged over the period 0700–1800 mountain standard time (MST). Also given are the daily soil moisture values estimated using gravimetric samples [*Schmugge et al.*, this issue] and the midday Bowen ratio, B_0 ($=H/LE$), averaged for the period 1030–1430 MST; during the experiment 1030 and 1430 MST were about 2 hours before and after solar noon, respectively. The average midday B_0 for the eight METFLUX sites on DOY 209 was 0.65 (±0.12), suggesting the vegetation was supplied with adequate moisture in the root zone. The average value of B_0 dropped on DOY 216 to about 0.36 (±0.09) as a result of the recent rains in the area, but increased on DOY 221 to approximately 0.8 (±0.20). Note that variations in B_0 and daily soil moisture values are the largest on DOY 221. In fact, a plot of surface soil moisture versus B_0 for DOY 216 and 221 (see Figure 5) suggests that there is a significant correlation between areas which maintained higher surface soil moisture after the rain events and lower B_0 values. However, this relationship is only applicable when spatial variation in near-surface soil moisture is dominating the energy flux contributions from the soil-vegetation system. This situation is most likely to occur during the initial drying phase of the near-surface soil, which is strongly coupled to the soil evaporation [*Mahrt and Pan*, 1984; *Mahfouf and Noilhan*, 1991]. A similar relationship for inferring trends in B_0 values over large areas may be acquired from a series of remotely sensed brightness temperature maps from a passive microwave instrument [see *Schmugge et al.*, this issue].

For this analysis the surface temperature and reflectance data were spatially averaged in order to represent pixel sizes ranging over several orders in magnitude. The number of observations that were averaged for representing various pixel sizes was estimated by assuming an aircraft speed of 50 m s^{-1} and multiplying by the required number of measurements (the data were sampled at 1 Hz) to produce the length scale needed. Since the area observed on the ground by the sensors was roughly 25 m × 25 m, the scaling up of pixel size was one dimensional, that is, along the flight path. The actual airplane speed varied; however, an average for 24 flight lines gave about 50 m s^{-1} (±10 m s^{-1}). Therefore data averaged for several observations around each METFLUX site were assumed to represent a 200-m pixel. This was scaled up to an average of 20 observations or a 1-km pixel, an average of 40 observations or a 2-km pixel, and finally a mean for the whole flight line producing a pixel of order 10 km.

The results of this averaging technique for the thermal-infrared observations for all three days are illustrated in Figure 6. Standard deviations of T_s values averaged over the total length of the flight lines were around ±1.5°C. Differences in T_s values for a given site averaged over 0.2-km, 1-km, and 2-km length scales were normally smaller than 1.5°C. Note that there are only a few cases where any of the integrated values for a given site fall outside one standard deviation of the T_s value for the 10-km pixel. The largest variation in T_s is observed on DOY 216 for line 2 during the 1130 MST overflight. The most likely cause for this relatively large variation in T_s is nonuniform radiation loading over the sites due to clouds. This variation in radiation is easily illustrated in Figure 7 where interpolated values (using the mean overflight time for lines 1 or 2 illustrated in Figure 1) of

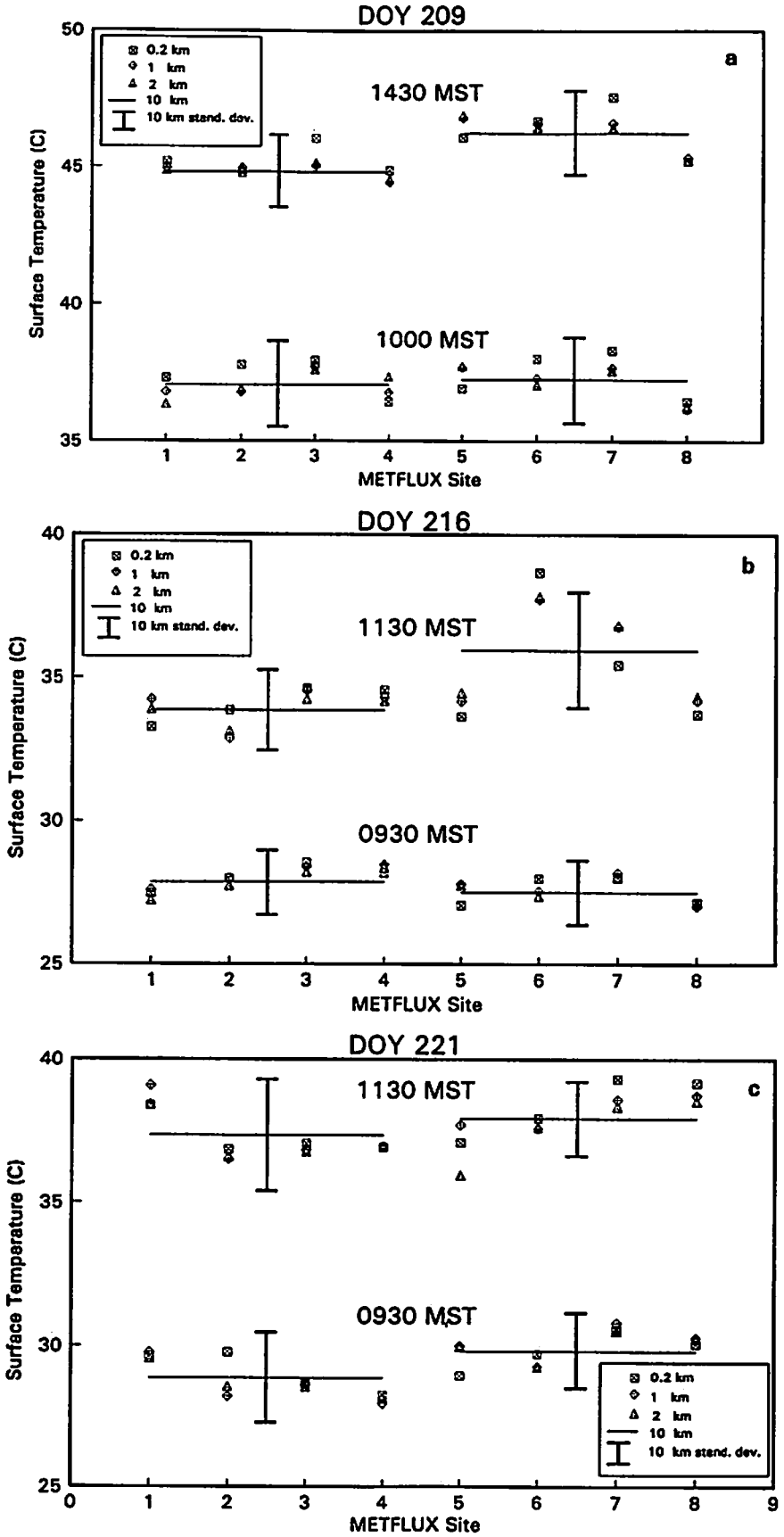

Figure 6. Surface temperatures averaged from aircraft observations made on (a) DOY 209, (b) DOY 216, and (c) DOY 221. The mean values consist of averaging multiple observations that represent pixels of order 0.2 km, 1 km, 2 km, and 10 km. The vertical bars represent standard deviations for the 10-km pixel data.

Table 4. Estimates of z_{om}, and d_{0m} Employed in Model Calculations

METFLUX Site	z_{0m}, m	d_{0m}, m
1	0.04	0.5
2	0.04	0.5
3	0.04	0.5
4	0.01	0.3
5	0.01	0.3
6	0.03	0.3
7	0.03	0.5
8	0.05	0.5

the 20-min R_{si} means at each site are plotted for the three days.

As outlined above (see the model section), the local roughness lengths for the METFLUX sites were determined by several approaches [*Kustas et al.*, this issue]. The values of z_{0m} and d_{0m} used with the remote sensing model for computing the local energy fluxes are given in Table 4.

For the regional or effective roughness length Z_{0m}, (17)–(19) were employed with several estimates of h and λ determined from general topographic information given by *Kustas and Goodrich* [this issue]. Stated briefly, the main drainage channels run approximately from northeast to southwest (~220° from north) with distances between ridgetops (perpendicular to the drainage) typically of order 500 m and heights from valley floor to ridgetop normally between 10 and 15 m. The value of z_{0m}, representing in the regional roughness equations the surface roughness without any topography, was estimated from the results in Table 4. The computed values of Z_{0m} are listed in Table 5. With the range of input data, (17)–(19) suggest that $Z_{0m} \sim 0.10$–0.20 m. A value of D_{0m} was estimated by simply taking half the height the obstacles, yielding $D_{0m} \sim 5$ m. The sensitivity of model output to the estimate of D_{0m} is negligible since the tops of convective mixed layers, H_i, are typically of the order of 10^3 m (see Table 6).

Free soundings of the ABL were available for each day with aircraft missions. The soundings taken within 30 min of the aircraft mission were used with (13)–(16) for computing regional energy fluxes. Estimates of the mixed layer height, H_i, and Θ_a came from the potential temperature profile while U came from averaging the wind speeds over the same mixed layer region. Figure 8 shows an example of this averaging process for one of the soundings, and Table 6 lists estimates of the parameters required in (13)–(16). Note that only a late morning sounding was available for DOY 216, so the remote sensing data collected in the morning could not be used for regional flux calculations.

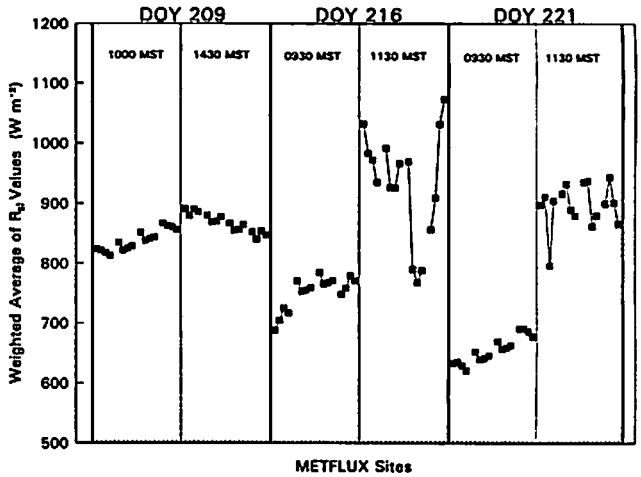

Figure 7. Weighted average of the 20-min R_{si} values surrounding aircraft flight times over METFLUX sites. For each flight the order of sites shown is 5–8 (line 2), 1–4 (line 1), 4–1 (line 1), and 8–5 (line 2).

For the local fluxes, meteorological data for each METFLUX site were interpolated to match the overflight time. There was some variation in fluxes among the sites which was due to differences in overpass times between lines 1 and 2, but the strongest effect appeared to be due to radiation. This is clearly seen by comparing the standard deviations of the energy fluxes averaged for the eight METFLUX sites listed in Table 7. On DOY 216 the 1130 MST overflight (mean time for lines 1 and 2) had the largest variation in the fluxes caused by cloudiness (Figure 7). This appears to override the spatial variation in Bowen ratio or soil moisture conditions evident on DOY 221 (Table 3).

An average of the energy balance components for all eight METFLUX sites in Table 7 was assumed to be representative of the regional scale fluxes. A simple average to represent regional fluxes was deemed appropriate for the days and wind directions considered. However, this approach may not be suitable if there is a significant variation in the surface energy balance upwind of the METFLUX network. For example if there was an anomaly in soil moisture which covered an area $\sim 10^2$ km^2 upwind of the study site the ABL may not represent area-averaged fluxes from the METFLUX network [*Shuttleworth*, 1988]. Furthermore, regional fluxes cannot be estimated when the atmospheric flow is such that the area significantly contributing to the regional fluxes is not well represented by the area where fluxes are being measured and the remote sensing data are being collected [e.g., *Schuepp et al.*, 1990]. For DOY 209 the atmospheric flow was from the north-northwest; hence, the

Table 5. Estimates of the Effective or Regional Roughness Length, Z_{0m}, Using Gross Terrain Features With Semiempirical Equations

Mean Obstacle Height h, m	Distance Between Obstacles λ, m	Roughness Length With No Topography, m	Value From Equation (18) [*Emeis*, 1987], m	Value From Equation (19) [*Lettau*, 1969], m	Value From Equation (17) [*Taylor et al.*, 1989], m
10	500	0.03	0.07	0.10	0.05
15	500	0.03	0.10	0.23	0.10

Table 6. Processed Atmospheric Boundary Layer Data Used in Model Calculations of Regional Energy Fluxes

DOY	Time, MST	H_i, m	θ_a, K	U, m s^{-1}	Wind Direction,* deg from N
209	1030	950	313	3.0	315
209	1600	1550	316.3	7.0	320
216	1150	1680	313	3.4	104
221	0930	970	309.6	6.7	97
221	1115	1440	310.5	7.7	99

*Wind direction is averaged over the same height range used in estimating U.

upwind fetch was mainly from outside the METFLUX network and the remote sensing transects. Nevertheless, the dry soil surface and clear sky conditions in the study area were typical of the surrounding region and therefore were assumed to be representative. For DOY 216 the soil moisture and meteorological conditions were heterogeneous due to the high spatial variability in rainfall and cloud cover, but the ABL flow was from the east, yielding an upwind fetch

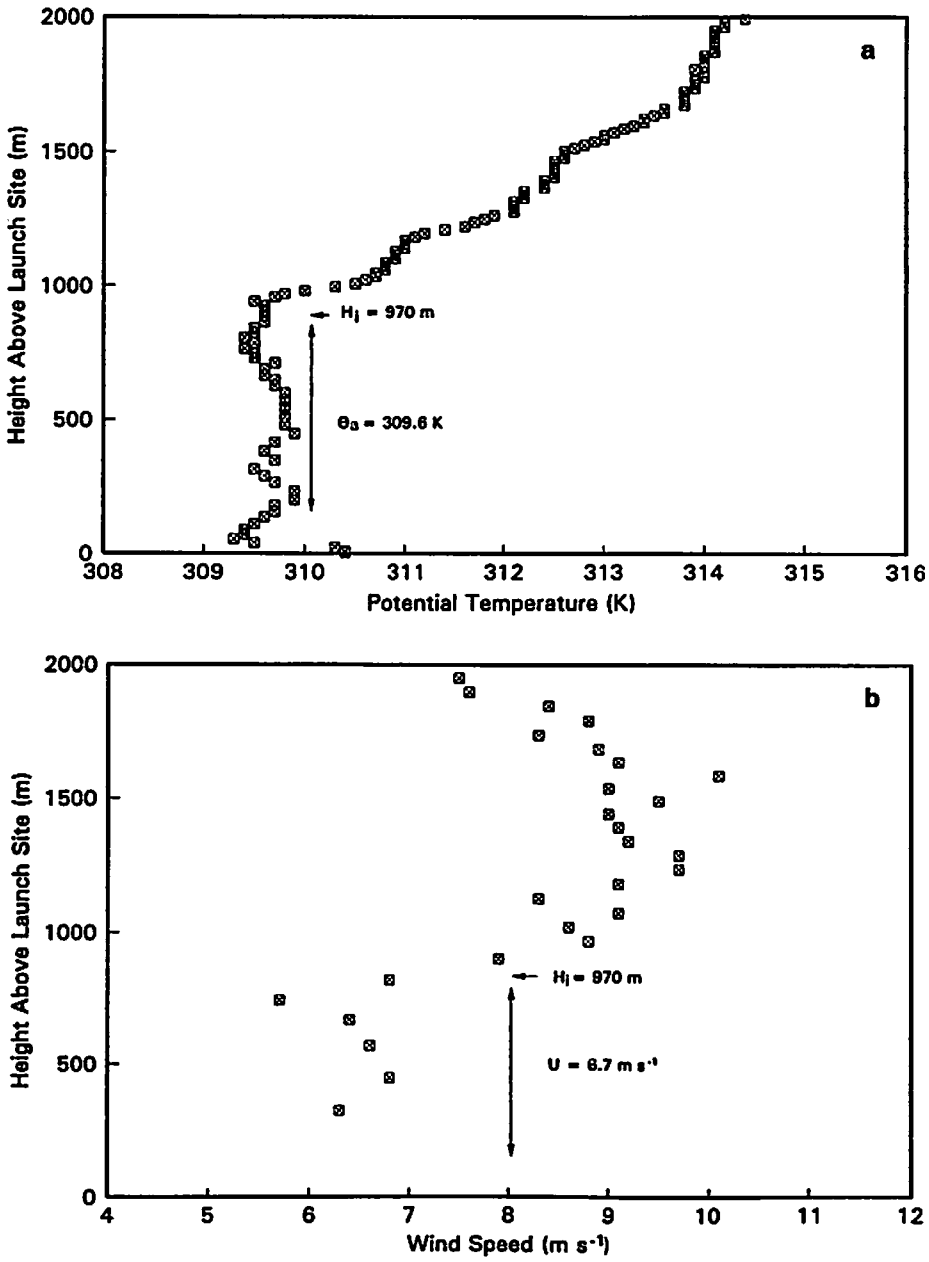

Figure 8. An example of estimating mixed layer variables from (a) the potential temperature profile and from (b) the wind speed data used in the bulk ABL resistance model. Data are from sounding on DOY 221 at about 0930 MST (see Table 6).

Table 7. Average and (Standard Deviation) of the Energy Balance Components Given by the METFLUX Network for the Period Covering Remote Sensing Data Acquisition Over Flight Lines 1 and 2

DOY	Time, MST	R_{si}, W m^{-2}	R_n, W m^{-2}	G, W m^{-2}	H, W m^{-2}	LE, W m^{-2}
209	1011	838 (±18)	512 (±33)	−154 (±25)	−121 (±16)	−237 (±35)
209	1430	868 (±16)	506 (±29)	−113 (±14)	−158 (±17)	−235 (±38)
216	0930	752 (±28)	506 (±31)	−162 (±28)	−91 (±17)	−252 (±27)
216	1115	933 (±91)	625 (±80)	−181 (±21)	−123 (±29)	−321 (±80)
221	0913	656 (±23)	423 (±30)	−121 (±24)	−111 (±17)	−192 (±31)
221	1113	898 (±37)	587 (±41)	−171 (±24)	−182 (±24)	−234 (±39)

which integrated over an area covering the METFLUX network and the remote sensing transects. For DOY 221 the upwind fetch was also from the east, again providing an ABL whose properties were representative of environmental conditions measured within the study area.

Model Results and Discussion

A statistical analysis by which the model calculations using local meteorological data together with the remote sensing observations representing 0.2-km, 1-km, and 2-km pixels are compared to the local fluxes measured at the METFLUX sites is presented in Table 8. Evaluation of the difference between modeled and measured fluxes is given by the root mean square error (RMSE), shown to be a better indicator of model performance than correlation statistics [*Willmott*, 1982], and by mean absolute difference (MAD) and mean absolute percent difference (|MPD|). The statistical results are given for each day and also for the three days combined. The differences between modeled and measured fluxes do not change significantly as a function of the pixel size. The largest differences in the flux estimates occurred on DOY 216, which had the largest variability in radiation fluxes (see Figure 7) and in the remotely sensed data (see Figures 3b and 6b). A plot of model versus measured energy balance components is given in Figure 9 using the 1-km pixel data. Figures 9a and 9b show generally satisfactory agreement between measured and remote estimates of R_n and G with no significant bias. However, the model tends to overestimate G when measured values ranged from 100 to 150 W m^{-2} (see Figure 9b). Overall, the results imply that local measurements of available energy at the METFLUX sites can at times be representative of a significantly larger area. Figure 9c reveals a tendency for model calculations to underestimate measured H, yet this tendency does not appear to produce a similar bias when comparing the LE values (Figure 9d). This is due, in part, to the overestimates of G by the remote method compensating for many of the cases when the model underestimates H. Hence the residual calculations may agree well with observations, but contain compensating errors in the other energy balance terms.

The expression for determining the difference in roughness length of heat versus momentum via the kB^{-1} expression given by (12) was evaluated in another brush-dominated semiarid region [*Kustas et al.*, 1989b]. For that region the

Table 8. Statistical Results Comparing Fluxes From METFLUX Sites With Model Estimates

Pixel Size, km	RMSE, W m^{-2}				MAD, W m^{-2}				|MPD|, %			
	R_n	G	H	LE	R_n	G	H	LE	R_n	G	H	LE
					DOY 209							
0.2	31	33	31	55	25	28	25	46	5	24	19	19
1	30	34	29	51	24	29	24	42	5	25	18	17
2	32	34	29	50	26	30	24	41	5	25	18	17
					DOY 216							
0.2	37	27	37	57	31	24	30	41	5	14	28	15
1	38	28	36	56	32	25	30	41	6	15	28	15
2	40	28	37	58	34	25	30	44	6	15	29	16
					DOY 221							
0.2	36	25	33	30	27	22	27	24	5	17	18	12
1	35	25	33	30	28	23	26	23	6	17	17	12
2	33	25	34	30	27	23	27	22	6	18	18	12
					All Days							
0.2	35	28	34	49	28	25	27	37	5	19	22	15
1	35	29	33	47	28	26	27	36	5	19	21	15
2	35	29	33	48	29	26	27	36	6	19	21	15

Calculations were performed with remote sensing data averaged to represent 0.2-km, 1-km, and 2-km pixels and with $s_{kB} = 0.17$ in (12).

Root mean square error, RMSE = $[\sum_{i=1}^{n} (X_i - Y_i)^2/n]^{1/2}$, mean absolute difference, MAD = $\sum_{i=1}^{n} | (X_i - Y_i) |/n$, and mean absolute percent difference |MPD| = $\sum_{i=1}^{n} (|(X_i - Y_i)|/|Y_i|)/n$, where Y_i represents H and LE estimated at the METFLUX site and X_i represents H and LE calculated by the model.

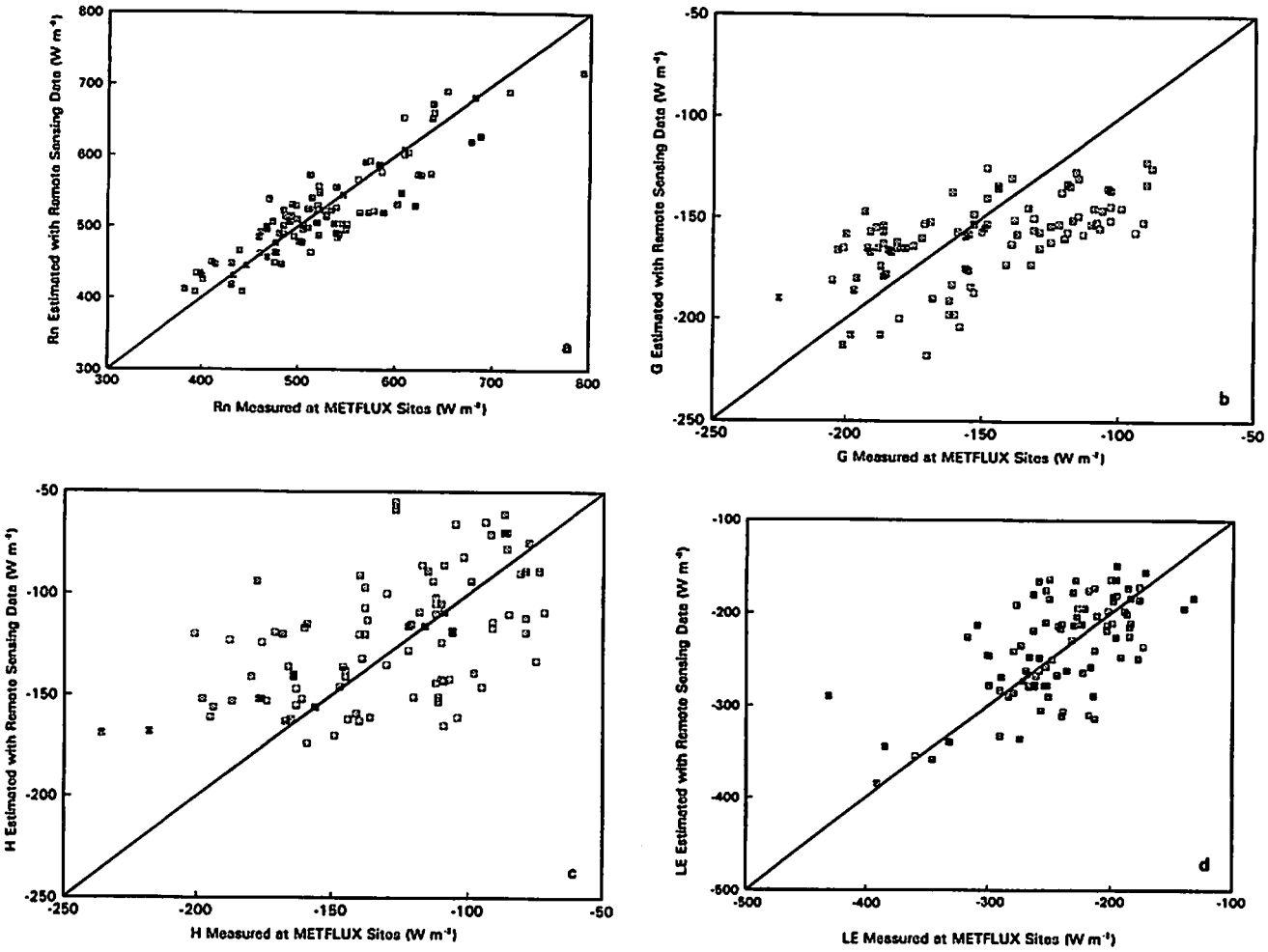

Figure 9. Comparison between model calculations and METFLUX estimates of (a) R_n, (b) G, (c) H, and (d) LE. The model results are shown using the 1-km pixel values and the meteorological data from the METFLUX sites. The model uses $s_{kB} = 0.17$ for computing the scalar roughness for heat (see text).

value of z_{0m} (~0.10 m) was estimated using *Lettau*'s [1969] expression for bluff body types of surfaces. Estimates of the momentum roughness parameters from the present study and others in semiarid ecosystems [e.g., *Weaver*, 1990] suggest that a smaller value of z_{0m} would probably be more appropriate, namely, of the order of 0.05 m. Use of a smaller z_{0m} value would reduce the slope, s_{kB}, of the kB^{-1} expression given by (12) because $kB^{-1} = \ln(z_{0m}/z_{0h})$. A rough approximation for computing the reduction in s_{kB} was performed by taking the ratio of the logarithm expression in (9), that is $\ln[(z - d_{0m})/z_{0m}]$, with $z_{0m} = 0.01$ m versus the more likely value of $z_{0m} = 0.05$ and $(z - d_{0m}) \sim 1$ m. The ratio yielded a reduction in slope of about 25% or $s_{kB} \approx 0.13$. The analysis with the local meteorological data and the integrated remote sensing observations (i.e., 0.2-km, 1-km, and 2-km pixel values) was performed with the smaller value of s_{kB} in (12). The results are listed in Table 9. Overall, differences between modeled and measured H and LE fluxes are slightly higher than the results using $s_{KB} = 0.17$ (see Table 8). The main reason for this is that the difference for DOY 209 is significantly increased compared to Table 9 while only marginal improvement is made for DOY 221. Comparison of modeled versus METFLUX values of H and LE using $s_{kB} = 0.13$ in (12) and the 1-km pixel data are shown in Figure 10. The computed H values from the model illustrated in Figure 10a show a strong tendency to overestimate the METFLUX measurements. This results in residual calculations of LE by the model that generally underestimate LE given by METFLUX sites (see Figure 10b). However, similar model comparisons with measured fluxes using ground-based remote sensing data collected at METFLUX sites 1 and 5 indicated that using $s_{kB} = 0.13$ gave slightly better results [*Moran et al.*, this issue].

Estimates of the regional energy fluxes with the ABL data and the remote sensing measurements averaged over 10 km were compared with the METFLUX averages given in Table 7. The statistical results using $Z_{0m} = 0.1$ m and 0.2 m and $s_{kB} = 0.17$ and 0.13 in (20) are listed in Table 10. The table shows that best overall results are obtained with $Z_{0m} = 0.1$ m and $s_{kB} = 0.17$. In Figure 11 the regional surface energy balance given by the average of the METFLUX network is compared to the ABL model calculations. Figures 11a and 11b show good agreement in the estimates of R_n and G, while Figures 11c and 11d support the statistical results in Table 10, namely, that better overall agreement is obtained for estimating the turbulent fluxes when $s_{kB} \sim 0.17$.

Table 9. Statistical Results Comparing Fluxes From METFLUX Sites With Model Estimates

Pixel Size, km	RMSE, W m^{-2}		MAD, W m^{-2}		|MPD|, %	
	H	*LE*	*H*	*LE*	*H*	*LE*
			DOY 209			
0.2	49	83	41	75	32	31
1	47	79	39	70	31	29
2	46	77	39	68	30	28
			DOY 216			
0.2	40	60	32	41	32	14
1	40	60	32	41	32	14
2	41	62	33	45	33	16
			DOY 221			
0.2	24	35	20	33	16	16
1	23	32	19	29	15	14
2	23	29	18	26	14	13
			All Days			
0.2	39	63	31	50	27	20
1	38	60	30	47	26	19
2	38	60	30	46	26	19

The remote sensing data were averaged in order to represent 0.2-km, 1-km, and 2-km pixels and the value of s_{kB} = 0.13 in (12). Only model calculations of *H* and *LE* are affected by changing the value of s_{kB}. RMSE, MAD, and |MPD| are defined in footnote to Table 8.

Conclusions

Estimates of the surface energy balance at length scales of the order of 10^0 km with a one-dimensional bulk resistance model designed to use local optical remote sensing observations and meteorological data agreed satisfactorily with values determined from the METFLUX sites. Differences were typically within the accuracy of the ground-based measurements (i.e., ~20%). Moreover, the model was adapted to utilize upper ABL data with large-scale remote sensing measurements (i.e., pixel size of order ~10^1 km), yielding regional scale fluxes. The comparison between the regional energy flux model and averages from the METFLUX network was similar to the results given by the local scale model. The emphasis in this study was to develop a procedure which minimized the number of model parameters and relied primarily on remotely sensed information and ancillary meteorological data for computing the fluxes. It was found that integrating up the remote sensing data to represent 0.2-km, 1-km, and 2-km pixels did not significantly change the average values of the remote sensing data nor the model output of the local fluxes. The strongest effect on the variability of remote sensing data, measured fluxes, and model output was the spatial variation in cloud cover, which resulted in significant differences in both modeled and measured energy fluxes among the sites.

While radiation, near-surface wind speed, air temperature measurements, and local roughness parameters were available for each METFLUX site, such a dense network is not

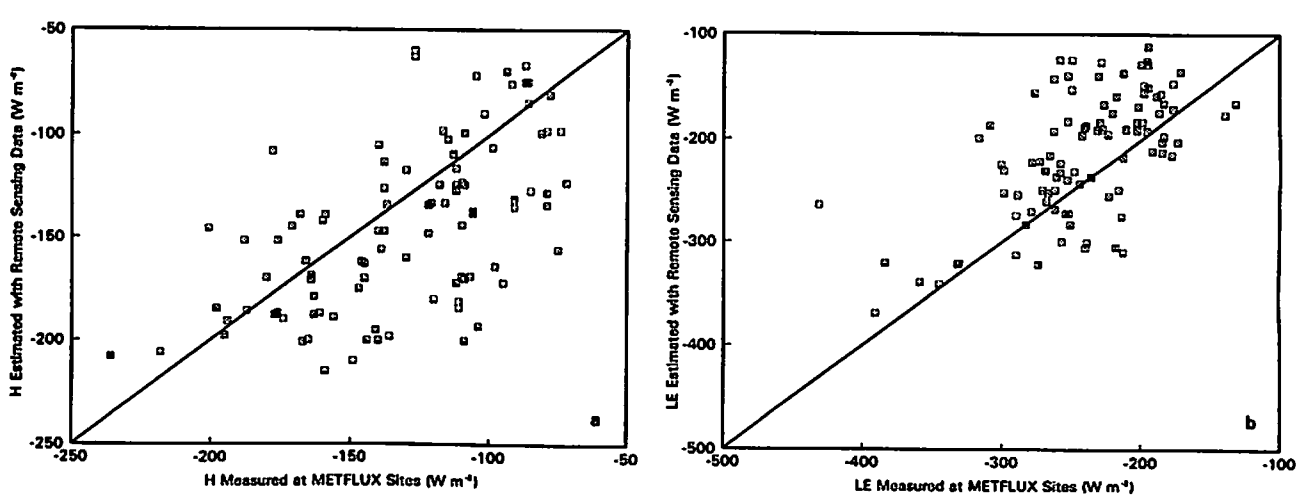

Figure 10. Same as Figure 9 for comparing (a) *H* and (b) *LE*, but s_{kB} = 0.13 for determining the scalar roughness for heat (see text).

Table 10. A Statistical Analysis of Regional Flux Estimates From the Model Using Atmospheric Boundary Layer and 10-km Pixel Data

		RMSE, W m^{-2}				MAD, W m^{-2}				|MPD|, %			
Z_{0m}	s_{kB}	R_n	G	H	LE	R_n	G	H	LE	R_n	G	H	LE
0.1	0.17	28	19	32	25	22	14	23	22	4	11	15	9
0.1	0.13	28	19	34	50	22	14	31	44	4	11	24	18
0.2	0.17	28	19	36	45	22	14	31	40	4	11	23	16
0.2	0.13	28	19	60	106	22	14	55	83	4	11	43	31

Average values from the METFLUX network were assumed to represent regional energy fluxes. RMSE, MAD, and |MPD| are defined in footnote to Table 8.

commonly available. Usually a meteorological station is located outside the area of interest and is representative of local environmental conditions. This makes it difficult to extrapolate model calculations to other areas where there may be significantly different meteorological and surface roughness conditions. However, remote sensing data can be used to quantify some of the changes in the surface energy balance components caused by spatial variation in surface conditions, including surface temperature, albedo, and vegetation cover. In the work by *Humes et al.* [this issue (a)] a simple remote sensing model for extrapolating energy fluxes from one location shows some promise. But spatial variation in incoming solar radiation, meteorological conditions, and surface roughness cannot be accounted for by the model, which can lead to significant variation in the fluxes.

Efforts that utilize geostationary satellite systems for computing large-area estimates of radiation yield reliable results [*Pinker et al.*, this issue]. Moreover, the use of the bulk similarity theory of the ABL with the semiempirical techniques for estimating the roughness parameters for

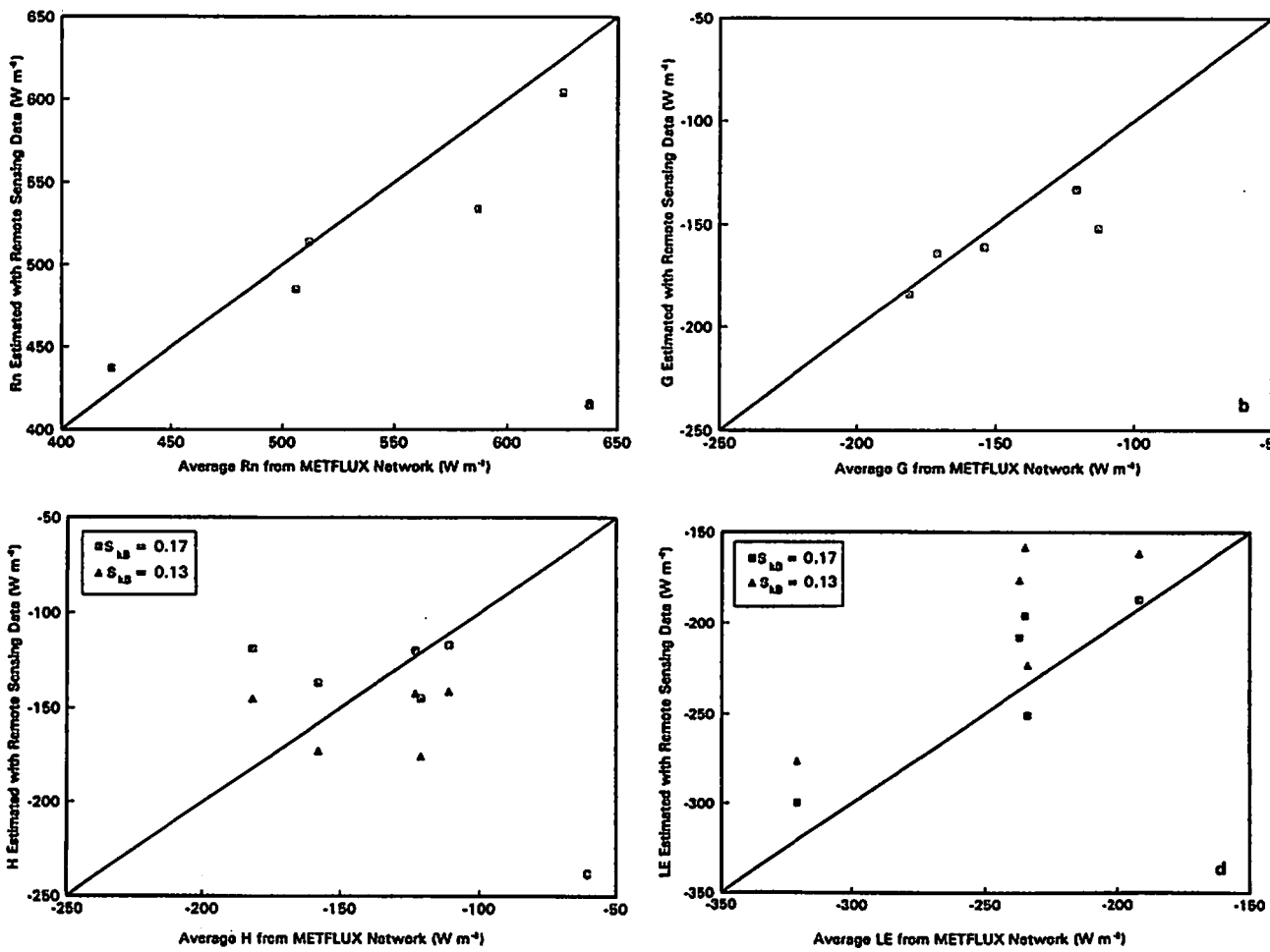

Figure 11. Regional scale estimates of the surface energy balance using the bulk ABL resistance model with mixed layer potential temperature and wind speed and 10-km pixel data versus averages from the METFLUX network of (a) R_n, (b) G, (c) H, and (d) LE. For H and LE comparisons, model results are shown with s_{kB} = 0.17 and s_{kB} = 0.13 in (20).

momentum and heat appears to be applicable to complex surfaces. Therefore by quantifying regional scale fluxes some of the problems associated with variation in local energy balance components are avoided. The relative simplicity of the model makes it useful to compare with output from more sophisticated prognostic models simulating regional scale surface-atmospheric energy flux exchange over time [e.g., *Avissar and Pielke*, 1989; *Lagouarde and Brunet*, 1989] when remotely sensed data are available.

More work is needed to test the reliability of the methods used in estimating key model input variables and parameters. The key model parameters include the local and regional momentum roughness and the scalar roughness for heat evaluated by (12) and (20). The stability of the coefficient s_{kB} has to be evaluated over different surfaces. If the coefficient is highly variable, it must be determined whether remote sensing information can be used to infer its value. The likely errors in the remotely sensed variables (i.e., surface temperature, visible and near-IR reflectances) and associated model sensitivity to the calculated fluxes need further study. The errors in remotely sensed variables from satellite platforms would be of special concern if the model were to be used operationally for evaluating regional energy fluxes.

Acknowledgments. This study would not have been possible without the cooperation and assistance of the USDA ARS Tombstone Laboratory personnel: Howard Larsen, Art Dolphin, John Smith, and Jim Smith. Also the assistance of USDA ARS Southwest Watershed Research Center is greatly appreciated. Finally, this project would not have been conducted without the financial support of the NASA Interdisciplinary Research Program in the Earth Sciences (NASA reference number IDP-88-086) and from USDA ARS Beltsville Area funds.

References

André, J.-C., J.-P. Goutorbe, and A. Perrier, HAPEX-MOBILHY: A Hydrologic Atmosphere Experiment for the study of water budget and evaporation flux at the climatic scale, *Bull. Am. Meteorol. Soc.*, *67*, 138–144, 1986.

André, J.-C., P. Bougeault, and J.-P. Goutorbe, Regional estimates of heat and evaporation fluxes over non-homogeneous terrain: Examples from the HAPEX-MOBILHY Programme, *Boundary Layer Meteorol.*, *50*, 77–108, 1990.

Avissar, R., and R. A. Pielke, A parameterization of heterogeneous land surfaces for atmospheric numerical models and its impact on regional meteorology, *Mon. Weather Rev.*, *117*, 2113–2136, 1989.

Beljaars, A. C. M., The derivation of fluxes from profiles in perturbed areas, *Boundary Layer Meteorol.*, *24*, 35–55, 1982.

Beljaars, A. C. M., and A. A. M. Holtslag, Flux parameterization over land surfaces for atmospheric models, *J. Appl. Meteorol.*, *30*, 327–341, 1991.

Betts, A. K., R. L. Desjardins, J. I. Macpherson, and R. D. Kelly, Boundary-layer heat and moisture budgets from FIFE, *Boundary Layer Meteorol.*, *50*, 109–138, 1990.

Brest, C. L., and S. N. Goward, Deriving surface albedo measurements from narrow band satellite data, *Int. J. Remote Sens.*, *8*, 351–367, 1987.

Brunet, Y., K. T. Paw U, and L. Prevot, Using the radiative surface temperature in energy budget studies over plant canopies, Proceedings of the 5th International Colloquium Physical Measurements and Signatures in Remote Sensing Courchevel, France, *Eur. Space Agency Spec. Publ. ESA SP-319*, 557–560, 1991.

Brutsaert, W., On a derivable formula for long-wave radiation from clear skies, *Water Resour. Res.*, *11*, 742–744, 1975.

Brutsaert, W. H., *Evaporation into the Atmosphere*, 199 pp., D. Reidel, Norwell, Mass., 1982.

Brutsaert, W., and M. Sugita, The extent of the unstable Monin-Obukhov layer for temperature and humidity above complex hilly grassland, *Boundary Layer Meteorol.*, *51*, 383–400, 1990.

Brutsaert, W., and M. Sugita, A bulk similarity approach in the atmosphere boundary-layer using radiometric skin temperature to determine regional surface fluxes, *Boundary Layer Meteorol.*, *55*, 1–12, 1991.

Brutsaert, W., and M. Sugita, Regional surface fluxes from satellite-derived surface temperatures (AVHRR) and radiosonde profiles, *Boundary Layer Meteorol.*, *58*, 355–366, 1992.

Camillo, P., Estimating soil surface temperatures from profile temperature and flux measurements, *Soil Sci.*, *148*, 233–243, 1989.

Camillo, P. J., R. J. Gurney, and T. J. Schmugge, A soil and atmospheric boundary layer model for evapotranspiration and soil moisture studies, *Water Resour. Res.*, *19*, 371–380, 1983.

Camuffo, D., and A. Bernardi, An observational study of heat fluxes and their relationships with net radiation, *Boundary Layer Meteorol.*, *23*, 359–368, 1982.

Carl, D. M., T. C. Tarbell, and H. A. Panofsky, Profiles of wind and temperature from towers over homogeneous terrain, *J. Atmos. Sci.*, *30*, 788–794, 1973.

Carlson, T. N., J. K. Dodd, S. G. Benjamin, and J. N. Cooper, Satellite estimation of the surface energy balance, moisture availability and thermal inertia, *J. Appl. Meteorol.*, *20*, 67–87, 1981.

Carlson, T. N., E. M. Perry, and T. J. Schmugge, Remote estimation of soil moisture availability and fractional vegetation cover for agricultural fields, *Agric. For. Meteorol.*, *52*, 45–69, 1990.

Chamberlain, A. C., Transport of gases to and from surfaces with bluff and wave-like roughness elements, *Q. J. R. Meteorol. Soc.*, *94*, 318–332, 1968.

Choudhury, B. J., S. B. Idso, and R. J. Reginato, Analysis of an empirical model for soil heat flux under a growing wheat crop for estimating evaporation by an infrared-temperature based energy balance equation, *Agric. For. Meteorol.*, *39*, 283–297, 1987.

Clothier, B. E., K. L. Clawson, P. J. Pinter, Jr., M. S. Moran, R. J. Reginato, and R. D. Jackson, Estimation of soil heat flux from net radiation during the growth of alfalfa, *Agric. For. Meteorol.*, *37*, 319–329, 1986.

Dyer, A. J., A review of the flux-profile relationships, *Boundary Layer Meteorol.*, *7*, 363–372, 1974.

Emeis, S., Pressure drag and effective roughness length with neutral stratifications, *Boundary Layer Meteorol.*, *39*, 379–401, 1987.

Fiedler, F., and H. A. Panofsky, The geostrophic drag coefficient and the effective roughness length, *Q. J. R. Meteorol. Soc.*, *98*, 213–220, 1972.

Fuchs, M., and C. B. Tanner, Infrared thermometry of vegetation, *Agron. J.*, *58*, 597–601, 1966.

Garratt, J. R., and R. J. Francey, Bulk characteristics of heat transfer in the unstable, baroclinic atmospheric boundary layer, *Boundary Layer Meteorol.*, *15*, 399–421, 1978.

Garratt, J. R., and B. B. Hicks, Momentum, heat and water vapor transfer to and from natural and artificial surfaces, *Q. J. R. Meteorol. Soc.*, *99*, 680–687, 1973.

Garratt, J. R., J. C. Wyngaard, and R. J. Francey, Winds in the atmospheric boundary layer—Prediction and observation, *J. Atmos. Sci.*, *39*, 1307–1316, 1982.

Goodrich, D. C., T. J. Schmugge, T. J. Jackson, C. L. Unkrich, T. O. Keefer, R. Parry, L. B. Bach, and S. A. Amer, Runoff simulation sensitivity to remotely sensed initial soil water content, *Water Resour. Res.*, this issue.

Hipps, L. E., E. Swiatek, and W. P. Kustas, Interactions between regional surface fluxes and the atmospheric boundary layer over a heterogeneous watershed, *Water Resour. Res.*, this issue.

Högström, U., Non-dimensional wind and temperature profiles in the atmospheric surface layer: A re-evaluation, *Boundary Layer Meteorol.*, *42*, 55–78, 1988.

Huband, N. D. S., and J. L. Monteith, Radiative surface temperature and energy balance of a wheat canopy, I, Comparison of radiative and aerodynamic temperature, *Boundary Layer Meteorol.*, *36*, 1–17, 1986.

Huete, A. R., and R. D. Jackson, Suitability of spectral indices for evaluating vegetation characteristics on arid rangelands, *Remote Sens. Environ.*, *15*, 155–165, 1987.

Humes, K. S., W. P. Kustas, and M. S. Moran, Use of remote sensing and reference site measurements to estimate instantaneous surface energy balance components over a semiarid rangeland watershed, *Water Resour. Res.*, this issue (a).

Humes, K. S., W. P. Kustas, M. S. Moran, W. D. Nichols, and M. A. Weltz, Variability of emissivity and surface temperature over a sparsely vegetated surface, *Water Resour. Res.*, this issue (b).

Jackson, R. D., Evaluating evapotranspiration at local and regional scales, Proc. IEEE, *73*, 1086–1095, 1985.

Jackson, R. D., M. S. Moran, L. W. Gay, and L. H. Raymond, Evaluating evaporation from field crops using airborne radiometry and ground-based meteorological data, *Irrig. Sci.*, *8*, 81–90, 1987.

Jacquemin, N., and J. Noilhan, Sensitivity study and validation of a land-surface parameterization using HAPEX-MOBILHY data set, *Boundary Layer Meteorol.*, *52*, 93–134, 1990.

Kader, B. A., and A. M. Yaglom, Mean fields and fluctuation moments in unstably stratified turbulent boundary layers, *J. Fluid Mech.*, *212*, 637–662, 1990.

Kerr, Y. H., E. Assad, J. P. Freleaud, J. P. Lagouarde, and B. Seguin, Estimation of evapotranspiration in the Sahelian zone by use of METEOSAT and NOAA AVHRR data, *Adv. Space Res.*, *7*, 161–164, 1987.

Kimes, D. S., Effects of vegetation canopy structure on remotely sensed canopy temperatures, *Remote Sens. Environ.*, *10*, 165–174, 1980.

Kimes, D. S., J. A. Smith, and K. J. Ranson, Vegetation reflectance measurement as a function of solar zenith angle, *Photogramm. Eng. Remote Sens.*, *46*, 1563–1573, 1980.

Klassen, W., and W. van den Berg, Evapotranspiration derived from satellite observed surface temperature, *J. Clim. Appl. Meteorol.*, *24*, 412–424, 1985.

Kneizys, F. E., E. P. Shettle, L. W. Abreu, J. H. Chetwynde, G. P. Anderson, W. O. Gallery, J. E. A. Selby, and S. A. Clough, Users guide to LOWTRAN 7, *Rep. AGFL-TR-88-0177*, 137 pp., Air Force Cambridge Res. Lab., Hanscom Air Force Base, Mass., Aug. 1988.

Korrell, A., H. A. Panofsky, and R. J. Rossi, Wind profiles at the Boulder tower, *Boundary Layer Meteorol.*, *22*, 295–312, 1982.

Kustas, W. P., Estimates of evapotranspiration with a one- and two-layer model of heat transfer over partial canopy cover, *J. Appl. Meteorol.*, *29*, 704–715, 1990.

Kustas, W. P., and W. Brutsaert, Wind profile constants in a neutral atmospheric boundary-layer over complex terrain, *Boundary Layer Meteorol.*, *34*, 35–54, 1986.

Kustas, W. P., and C. S. T. Daughtry, Estimation of the soil heat flux/net radiation ratio from spectral data, *Agric. For. Meteorol.*, *49*, 205–223, 1990.

Kustas, W. P., and D. C. Goodrich, Preface, *Water Resour. Res.*, this issue.

Kustas, W. P., R. D. Jackson, and G. Asrar, Estimating surface energy-balance components from remotely sensed data, in *Theory and Applications of Optical Remote Sensing*, edited by G. Asrar, pp. 604–627, John Wiley, New York, 1989a.

Kustas, W. P., B. J. Choudhury, M. S. Moran, R. J. Reginato, R. D. Jackson, L. W. Gay, and H. L. Weaver, Determination of sensible heat flux over sparse canopy using thermal infrared data, *Agric. For. Meteorol.*, *44*, 197–216, 1989b.

Kustas, W. P., M. S. Moran, R. D. Jackson, L. W. Gay, L. F. W. Duell, K. E. Kunkel, and A. D. Matthias, Instantaneous and daily values of the surface energy balance over agricultural fields using remote sensing and a reference field in an arid environment, *Remote Sens. Environ.*, *32*, 125–141, 1990.

Kustas, W. P., et al., An interdisciplinary field study of the energy and water fluxes in the atmosphere-biosphere system over semi-arid rangelands: Description and some preliminary results, *Bull. Am. Meteorol. Soc.*, *72*, 1683–1705, 1991.

Kustas, W. P., J. H. Blanford, D. I. Stannard, C. S. T. Daughtry, W. D. Nichols, and M. A. Weltz, Local energy flux estimates for unstable conditions using variance data in semiarid rangelands, *Water Resour. Res.*, this issue.

Lagouarde, J.-P., Use of NOAA data combined with an agrometeorological model for evaporation mapping, *Int. J. Remote Sens.*, *12*, 1852–1864, 1991.

Lagouarde, J.-P., and Y. Brunet, Spatial integration of surface latent heat flux and evaporation mapping, *Adv. Space Res.*, *9*, 259–264, 1989.

Lettau, H., Note on aerodynamic roughness parameter estimation on the basis of roughness element description, *J. Appl. Meteorol.*, *8*, 828–832, 1969.

Mahfouf, J. F., A numerical simulation of the surface water budget during HAPEX-MOBILHY, *Boundary Layer Meteorol.*, *53*, 201–222, 1990.

Mahfouf, J. F., and J. Noilhan, Comparative study of various formulations of evaporation from bare soil using in situ data, *J. Appl. Meteorol.*, *30*, 1354–1365, 1991.

Mahrt, L., and H. Pan, A two-layer model of soil hydrology, *Boundary Layer Meteorol.*, *29*, 1–20, 1984.

Mason, P. J., The formation of aerially-averaged roughness lengths, *Q. J. R. Meteorol. Soc.*, *114*, 399–420, 1988.

Menenti, M., and J. C. Ritchie, Estimation of effective aerodynamic roughness of Walnut Gulch watershed with laser altimeter measurements, *Water Resour. Res.*, this issue.

Monin, A. S., and A. M. Obukhov, Basic laws of turbulent mixing in the ground layer of the atmosphere, *Tr. Geofiz. Inst. Akad. Nauk SSSR*, no. 24(151), 163–187, 1954.

Monteith, J. L., *Principles of Environmental Physics*, 241 pp., Elsevier, New York, 1973.

Moran, M. S., R. D. Jackson, L. H. Raymond, L. W. Gay, and P. N. Slater, Mapping surface energy balance components by combining Landsat thematic mapper and ground-based meteorological data, *Remote Sens. Environ.*, *30*, 77–87, 1989.

Moran, M. S., W. P. Kustas, A. Vidal, D. I. Stannard, J. H. Blanford, and W. D. Nichols, Use of ground-based remotely sensed data for energy balance evaluation of a semiarid rangeland, *Water Resour. Res.*, this issue.

Nappo, C. J., Mesoscale flow over complex terrain during Eastern Tennessee Trajectory Experiment (ETTEX), *J. Appl. Meteorol.*, *16*, 1186–1196, 1977.

Nemani, R. R., and S. W. Running, Estimation of regional surface resistance to evapotranspiration from NDVI and thermal-IR AVHRR data, *J. Appl. Meteorol.*, *28*, 276–284, 1989.

Nieuwenhuis, G. J., E. H. Smidt, and H. A. M. Thunnissen, Estimation of regional evapotranspiration of arable crops from thermal infrared images, *Int. J. Remote Sens.*, *6*, 1319–1334, 1985.

Noilhan, J., J. C. Andre, P. Bougeault, J. P. Goutorbe, and P. Lacarrere, Some aspects of the HAPEX-MOBILHY Programme: The data base and the modeling strategy, *Surv. Geophys.*, *2*, 31–62, 1991.

Owe, M., and A. A. van de Griend, Daily surface moisture model for large area semi-arid land application with limited climate data, *J. Hydrol.*, *121*, 119–132, 1990.

Owen, P. R., and W. R. Thomson, Heat transfer across rough surfaces, *J. Fluid Mech.*, *15*, 321–334, 1963.

Parlange, M. B., and W. Brutsaert, Regional roughness of the Landes Forest and surface shear stress under neutral conditions, *Boundary Layer Meteorol.*, *48*, 69–81, 1989.

Paulson, C. A., The mathematical representation of wind speed and temperature profiles in the unstable atmospheric surface layer, *J. Appl. Meteorol.*, *9*, 857–861, 1970.

Perry, E. M., and M. S. Moran, An evaluation of atmospheric conditions of radiometric surface temperatures for a semiarid rangeland watershed, *Water Resour. Res.*, this issue.

Pinker, R. T., Satellites and our understanding of the surface energy balance, *Palaeogeogr. Palaeoclimatol. Palaeoecol.*, *82*, 321–342, 1990.

Pinker, R. T., W. P. Kustas, I. Laszlo, M. S. Moran, and A. R. Huete, Basin-scale solar irradiance estimates in semiarid regions using GOES 7, *Water Resour. Res.*, this issue.

Price, J. C., Estimation of regional scale evapotranspiration through analysis of satellite thermal-infrared data, *IEEE Trans. Geosci. Remote Sens.*, *GE-20*, 286–292, 1982.

Price, J. C., Using spatial context in satellite data to infer regional scale evapotranspiration, *IEEE Trans. Geosci. Remote Sens.*, *28*, 940–948, 1990.

Rambal, S., B. Lacaze, H. Mazurek, and G. Debussche, Comparison of hydrologically simulated and remotely sensed actual evapotranspiration from some Mediterranean vegetation formations, *Int. J. Remote Sens.*, *6*, 1475–1481, 1985.

Robinson, S. M., Computing wind profile parameters, *J. Atmos. Sci.*, *19*, 189–190, 1962.

Schmugge, T. J., F. Becker, and Z.-L. Li, Spectral emissivity variations observed in airborne surface temperature measurements, *Remote Sens. Environ.*, *35*, 95–104, 1991.

Schmugge, T. J., T. J. Jackson, W. P. Kustas, R. Roberts, R. Parry, D. C. Goodrich, S. A. Amer, and M. A. Weltz, Push broom

microwave radiometer observations of surface soil moisture in Monsoon '90, *Water Resour. Res.*, this issue.

Schuepp, P. H., M. Y. Leclerc, J. I. MacPherson, and R. L. Desjardins, Footprint prediction of scalar fluxes from analytical solutions of the diffusion equation, *Boundary Layer Meteorol.*, *50*, 355–373, 1990.

Seguin, B., E. Assad, J. P. Freteaud, J. Imbernon, Y. Kerr, and J. P. Lagouarde, Use of meteorological satellites for water balance monitoring in Sahelian regions, *Int. J. Remote Sens.*, *10*, 1101–1117, 1989.

Sellers, P. J., F. G. Hall, G. Asrar, D. E. Strebel, and R. E. Murphy, The first ISLSCP field experiment (FIFE), *Bull. Am. Meteorol. Soc.*, *69*, 22–27, 1988.

Sellers, P. J., S. I. Rasool, and H.-J. Bolle, A review of satellite data algorithms for studies of the land surface, *Bull. Am. Meteorol. Soc.*, *71*, 1429–1447, 1990.

Serafini, Y. V., Estimation of evapotranspiration using surface and satellite data, *Int. J. Remote Sens.*, *8*, 1547–1562, 1987.

Shuttleworth, J. W., Macrohydrology—The new challenge for process hydrology, *J. Hydrol.*, *100*, 31–56, 1988.

Stull, R. B., *An Introduction to Boundary Layer Meteorology*, 666 pp., Kluwer Academic, Norwell, Mass., 1988.

Sucksdorff, Y., and C. Ottle, Application of satellite remote sensing to estimate areal evapotranspiration over a watershed, *J. Hydrol.*, *121*, 321–333, 1990.

Sugita, M., and W. Brutsaert, Wind velocity measurements in the neutral boundary layer above hilly prairie, *J. Geophys. Res.*, *95*(D6), 7617–7624, 1990a.

Sugita, M., and W. Brutsaert, Regional surface fluxes from remotely sensed skin temperature and lower boundary layer measurements, *Water Resour. Res.*, *26*, 2937–2944, 1990b.

Taconet, O., R. Bernard, and D. Vidal-Madjar, Evapotranspiration over an agricultural region using a surface flux/temperature model based on NOAA-AVHRR data, *J. Clim. Appl. Meteorol.*, *25*, 284–307, 1986.

Taylor, P. A., R. I. Sykes, and P. J. Mason, On the parameterization of drag over small-scale topography in neutrally-stratified boundary-layer flow, *Boundary Layer Meteorol.*, *48*, 409–422, 1989.

Thom, A. S., Momentum, mass and heat exchange of vegetation, *Q. J. R. Meteorol. Soc.*, *98*, 124–134, 1972.

Thompson, R. S., Note on aerodynamic roughness length for complex terrain, *J. Appl. Meteorol.*, *16*, 1402–1403, 1978.

Tucker, C. J., Red and photographic infrared linear combinations for monitoring vegetation, *Remote Sens. Environ.*, *8*, 127–150, 1979.

Tucker, C. J., and P. J. Sellers, Satellite remote sensing of primary production, *Int. J. Remote Sens.*, *7*, 1395–1416, 1986.

Tueller, P. T., and S. G. Oleson, Diurnal radiance and shadow fluctuations in a cold desert shrub plant community, *Remote Sens. Environ.*, *29*, 1–13, 1989.

Walthall, C. L., J. M. Norman, J. M. Welles, G. Campbell, and B. L. Blad, Simple equation to approximate bidirectional reflectance from vegetative canopies and bare soil surfaces, *Appl. Opt.*, *24*, 382–387, 1985.

Weaver, H. L., Temperature and humidity flux-variance relations determined by one-dimensional eddy correlation, *Boundary Layer Meteorol.*, *53*, 77–91, 1990.

Weltz, M. A., J. C. Ritchie, and H. D. Fox, Comparison of laser and field measurements of vegetation height and canopy cover, *Water Resour. Res.*, this issue.

Wieringa, J., Representativeness of wind observation at airports, *Bull. Am. Meteorol. Soc.*, *61*, 962–971, 1980.

Wieringa, J., Roughness-dependent geographical interpolation of surface wind speed averages, *Q. J. R. Meteorol. Soc.*, *112*, 867–889, 1986.

Willmott, C. J., Some comments on the evaluation of model performance, *Bull. Am. Meteorol. Soc.*, *63*, 1309–1313, 1982.

D. C. Goodrich, USDA ARS, Southwest Watershed Research Center, 2000 East Allen Road, Tucson, AZ 85719.

L. E. Hipps and E. Swiatek, Department of Plants, Soils, and Biometeorology, Utah State University, Logan, UT 84322-4820.

K. S. Humes and W. P. Kustas, USDA ARS, Hydrology Laboratory, Beltsville, MD 20705.

M. S. Moran and P. J. Pinter, Jr., USDA ARS, U.S. Water Conservation Laboratory, 4331 East Broadway Road, Phoenix, AZ 85040.

D. I. Stannard, Water Resources Division, U.S. Geological Survey, Mail Stop 413, Box 25046, Denver Federal Center, Denver, CO 80225.

(Received August 13, 1992; revised May 19, 1993; accepted October 19, 1993.)